https://doi.org/10.1093/plcell/koac301 THE PLANT CELL 2023: 35: 469–487

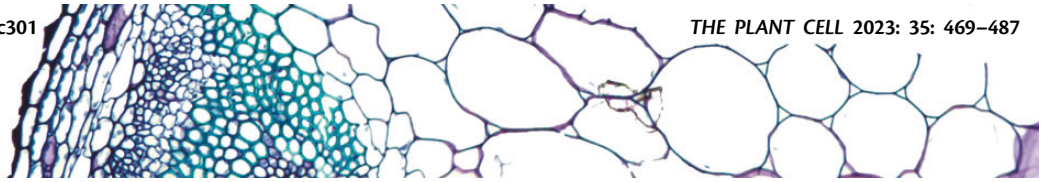

Research Article

Polarly localized WPR proteins interact with PAN receptors and the actin cytoskeleton during maize stomatal development

Qiong Nan [1], Si Nian Char [2], Bing Yang [3], Eric J. Bennett [3], Bing Yang [2,4] and Michelle R. Facette [1,*]

1 Department of Biology, University of Massachusetts, Amherst, Massachusetts 01003, USA
2 Division of Plant Sciences, Bond Life Sciences Center, University of Missouri, Columbia, Missouri 65211, USA
3 University of CaliforniaUniversity of California, San Diego, Department of Cell and Developmental Biology, La Jolla, California 92093, USA
4 Donald Danforth Plant Science Center, St Louis, Missouri 63132, USA

*Author for correspondence: mfacette@umass.edu

M.F. and Q.N. designed and performed the research, analyzed the data, and wrote the manuscript. B.Y. (UCSD) and E.J.B. performed the mass spectrometry for the initial set of co-IPs. S.N.C. and B.Y. (MO) designed the WPR CRISPR sgRNAs and prepared the constructs for maize transformation.
The author responsible for distribution of materials integral to the findings presented in this article in accordance with the policy described in the Instructions for Authors (https://academic.oup.com/plcell) is: Michelle Facette (mfacette@umass.edu).

Abstract

Polarization of cells prior to asymmetric cell division is crucial for correct cell divisions, cell fate, and tissue patterning. In maize (*Zea mays*) stomatal development, the polarization of subsidiary mother cells (SMCs) prior to asymmetric division is controlled by the BRICK (BRK)–PANGLOSS (PAN)–RHO FAMILY GTPASE (ROP) pathway. Two catalytically inactive receptor-like kinases, PAN2 and PAN1, are required for correct division plane positioning. Proteins in the BRK–PAN–ROP pathway are polarized in SMCs, with the polarization of each protein dependent on the previous one. As most of the known proteins in this pathway do not physically interact, possible interactors that might participate in the pathway are yet to be described. We identified WEAK CHLOROPLAST MOVEMENT UNDER BLUE LIGHT 1 (WEB1)/PLASTID MOVEMENT IMPAIRED 2 (PMI2)-RELATED (WPR) proteins as players during SMC polarization in maize. WPRs physically interact with PAN receptors and polarly accumulate in SMCs. The polarized localization of WPR proteins depends on PAN2 but not PAN1. CRISPR–Cas9-induced mutations result in division plane defects in SMCs, and ectopic expression of WPR-RFP results in stomatal defects and alterations to the actin cytoskeleton. We show that certain WPR proteins directly interact with F-actin through their N-terminus. Our data implicate WPR proteins as potentially regulating actin filaments, providing insight into their molecular function. These results demonstrate that WPR proteins are important for cell polarization.

Introduction

Asymmetric cell division, which generates two daughter cells with different fates, is indispensable for cellular differentiation and diversity. In plants, cells do not move; therefore, asymmetric cell division is particularly important for cellular patterning (De Smet and Beeckman, 2011; Muroyama and Bergmann, 2019; Shao and Dong, 2017; Pillitteri and Torii, 2012). Certain processes are conserved during asymmetric cell division, although the specific molecular players may

Received April 23, 2022. Accepted October 05, 2022. Advance access publication October 13, 2022

IN A NUTSHELL

Background: Stomata are small pores on the plant surface that open and close to allow gas exchange—allowing plants to "breathe". Plant species have different numbers, shapes, and arrangements of stomatal cells. In maize (*Zea mays*), stomata consist of two guard cells flanked by two subsidiary cells. Subsidiary cells are formed by an asymmetric division. Asymmetric cell divisions occur when a mother cell divides to give two cells that have different sizes, shapes, and/or functions—in this case, a specialized subsidiary cell and a generic pavement cell. The asymmetric division of the subsidiary mother cell (SMC) is a model to understand how plants regulate asymmetric divisions, which are important for forming different cell types. This division is regulated by several proteins that are unevenly distributed (polarized) in the mother cells prior to the division, including two receptors, PAN1 and PAN2.

Question: What proteins work together with PAN1 and PAN2 during maize SMC polarization? What cellular and molecular processes are important for maize subsidiary cell formation, and asymmetric divisions in general?

Findings: We found that members of the WPR protein family physically interact with PAN receptors. WPRs polarly localize in SMCs before division, and this polarization depends on PAN2 but not PAN1. When WPR proteins are missing, or there are increased levels of WPR proteins, subsidiary cells do not form properly. WPR proteins directly bind to the cytoskeleton—specifically F-actin. In fact, markers that label the actin cytoskeleton are altered when a WPR protein is overexpressed in maize.

Next step: Since the localization of WPRs depends on PAN2, but not PAN1, the relationship between the two different receptors and WPRs may differ. Understanding how PAN2 recruits WPRs to their location, or additional proteins that interact with WPRs will help us understand the function of the proteins in the pathway. In particular, how WPRs might regulate actin filament dynamics will provide an understanding of the function of WPR proteins in polarity, and in general.

vary. A key principle of asymmetric cell division is cell polarization prior to mitosis, which is often marked by the polarization of plasma membrane-associated proteins and nuclear migration to the future division plane (Galatis and Apostolakos, 2004; Facette and Smith, 2012; Yoshida et al., 2019). Cell polarization may be determined by intrinsic cues (pre-existing within the mother cell) or extrinsic cues (originating from outside the mother cell; Yang 2008; Lipka et al., 2015; Facette et al., 2019).

The asymmetric division of maize (*Zea mays*) subsidiary mother cells (SMCs) has been used as a model to understand cell polarization and asymmetric division in plants. Grasses such as maize, rice (*Oryza* spp.), and purple false brome (*Brachypodium distachyon*) possess four-celled stomatal complexes consisting of two guard cells flanked by a pair of subsidiary cells (Supplemental Figure S1). Grass stomatal formation is initiated by an asymmetric division that generates a guard mother cell (GMC). The lateral neighbors of the GMC, called SMCs, divide asymmetrically to produce subsidiary cells that flank the GMC. It is proposed that SMC divisions are induced by an extrinsic cue from the GMC. Eventually, the GMC divides symmetrically to form a pair of guard cells flanked by the subsidiary cells (Stebbins and Shah, 1960; Facette and Smith, 2012; Raissig et al., 2017; Nunes et al., 2020; Gray et al., 2020).

In maize SMCs, several plasma membrane-associated proteins make up the BRICK (BRK)–PANGLOSS (PAN)–RHO FAMILY GTPASE (ROP) pathway, which promotes SMC polarity. BRK1 is the earliest marker of SMC polarity (Facette et al., 2015). BRK1 is a member of the SCAR/WAVE complex that promotes branched actin networks via activation of the Arp2/3 complex (Frank and Smith 2002; Facette et al., 2015). BRK1, and all subsequent proteins, are polarized within SMCs, accumulating at the site of GMC contact. BRK1 is required for PAN2 and PAN1 polarization, which are two leucine-rich repeat receptor-like proteins (LRR-RLPs) with inactive kinase domains. PAN2 is required for the subsequent polarization of PAN1 (Zhang et al., 2012). Plant ROP is a small GTPase that physically interacts with PAN1; its polarization is dependent on PAN1 (Humphries et al., 2011). After the polarized accumulation of these proteins, an actin patch appears at the SMC–GMC interface and the pre-mitotic SMC nucleus migrates toward the GMC. Within the pathway, only PAN1 and ROP have been shown to physically interact; however, each protein is required for the next to be polarized. This implies that there are additional proteins important for the recruitment and/or polarization of each of the known players. Moreover, the molecular role that each of these proteins performs during SMC polarization is not known, including how polarization of these membrane-localized proteins culminates in nuclear migration and positioning of the division plane.

Since PAN1 and PAN2 are catalytically inactive kinases (Humphries et al., 2011; Zhang et al., 2012), it is unclear what their molecular function is. They may act as pseudokinases with important roles in scaffolding; however, other than ROP, no other PAN-interacting proteins have yet been characterized. In some cases, catalytically inactive receptors

partner with active leucine-rich repeat receptor kinases and act as inhibitors of function (Lee et al., 2012), but to date no active kinases have been identified in the pathway. PAN1 and PAN2 might perform functions similar to other polarized plasma membrane proteins and mediate diverse downstream functions that relate to cellular polarization such as signal transduction, accumulation of other cell polarity factors, or eventual nuclear migration (De Smet and Beeckman, 2011; Ashraf and Facette, 2020). For example, in Arabidopsis (*Arabidopsis thaliana*) stomatal development, the polarized proteins BREAKING OF ASYMMETRY IN THE STOMATAL LINEAGE (BASL) and POLAR LOCALIZATION DURING ASYMMETRIC DIVISION AND REDISTRIBUTION (POLAR) act as scaffolding proteins for localized signal transduction (Dong et al., 2009; Pillitteri et al., 2011; Houbaert et al., 2018). Notably, the *B. distachyon* ortholog of POLAR was recently discovered to have a distinct localization pattern during grass stomatal development that is opposite that of PAN1—it is excluded from the GMC–SMC contact site (Zhang et al., 2022). Polarized BASL is required for premitotic microtubule-based nuclear migration and postmitotic actin-based nuclear migration (Muroyama et al., 2020). The LRR-RLP INFLORESCENCE AND ROOT APICES RECEPTOR KINASE (IRK) is polarly localized in root cells that divide (or have recently divided) asymmetrically; however, the molecular pathway downstream of IRK is not characterized (Campos et al., 2020).

Polarized accumulation of actin filaments is a prominent feature of maize SMC division, but the functional role of the actin patch that forms late in SMC polarization is unclear. While SMC nuclear migration in grasses is based on actin networks (Kennard and Cleary, 1997; Cho and Wick, 1990), the formation of the actin patch and nuclear migration can be uncoupled (Cartwright et al., 2009; Apostolakos et al., 2018), implying that the actin patch has a function distinct from promoting nuclear migration. It is plausible that ROP GTPases are important for stimulating actin patch formation; however, this has not been clearly demonstrated. In addition to the actin patch, there are other important actin-related processes during SMC polarization. The early role of BRK proteins, actin-mediated nuclear migration and actin patch formation imply multiple functions for actin networks in SMC polarization. SMC actin filaments may provide force or/and tracks for polarized organelle movement, and/or may facilitate endo/exocytosis at the polarity site (Hadley et al., 2006; Kimata et al., 2016; Wu and Bezanilla, 2018).

Actin-dependent movement of chloroplasts has been shown to involve WEAK CHLOROPLAST MOVEMENT UNDER BLUE LIGHT 1 (WEB1) and PLASTID MOVEMENT IMPAIRED 2 (PMI2; Luesse et al., 2006; Kodama et al., 2010). WEB1, PMI2, and similar WEB1/PMI2-RELATED (WPR) proteins have a DUF827 domain which is a series of coiled-coils; *A. thaliana* has 14 DUF827-containing proteins including the WEB1-like (WEL) clade, PMI2-LIKE (PMI) clade, and WPRA and WPRB clades (Kodama et al., 2011). Previous studies in *A. thaliana* suggest that proteins with this domain have diverse functions. WEB1 and PMI2 are interacting proteins and are required for actin-based chloroplast photorelocation (Luesse et al., 2006; Kodama et al., 2010). TOUCH-REGULATED PHOSPHOPROTEIN1 (TREPH1) belongs to the WPRA protein clade and is phosphorylated in response to touch (Wang et al., 2018). TREPH1 is required for touch-induced growth repression. WEB1 is membrane-associated and PMI2 is cytosolic in protoplasts, but in planta localization for DUF827 proteins has not been demonstrated. Moreover, while the demonstrated phenotypes of WEB1 and PMI2 imply an actin-related function, no evidence for physical or regulatory interactions with actin have been shown for any DUF827 protein thus far.

In this study, we identified members of the DUF827 domain-containing WPR protein family that participate in maize SMC polarization. WPRs interact with both PAN2 and PAN1, and WPRs can also form homodimers and heterodimers. WPRs localize polarly in SMC at sites of GMC contact, and their polarized localization depends on PAN2 but not PAN1. These findings suggest that WPRs are plasma membrane-associated proteins that are important for premitotic polarity in maize SMCs and are the first physical link between PAN1 and PAN2. CRISPR–Cas9-induced *wprb1;wprb2* double mutants and plants ectopically expressing WPRB2 have an increased frequency of aberrantly formed subsidiary cells. WPRB2 overexpression causes a decrease in cellular F-actin signal, as indicated by a live fluorescent marker. Additionally, we show that WPRB2 directly interacts with F-actin through its N-terminus. In total, these results suggest that WPRs are components of the BRK–PAN–ROP pathway and likely act downstream of PAN2 to regulate actin-associated processes during cell polarization.

Results

WPRs exhibit polarized localization in maize SMCs

To better understand the functions of PAN and BRK proteins during SMC polarization, we identified proteins that physically interact with PAN2-YFP and PAN1-YFP. Co-immunoprecipitation/mass spectrometry (co-IP/MS) of BRK1-CFP, Rab11D-YFP, PIN1-YFP, PDI-YFP, and nontransgenic controls was previously performed using anti-GFP beads (Facette et al., 2015). In parallel, co-IP/MS of PAN2-YFP, and PAN1-YFP was also performed, but not presented in Facette et al. (2015). As previously published, a WD-score was calculated to identify high confidence interactors (Sowa et al., 2009; Facette et al., 2015). Amongst the PAN2-YFP interactors were four related proteins containing Domain of Unknown Function 827 (DUF827; Supplemental Data Set 1). The DUF827 family includes previously identified WEB1-PMI2-RELATED (WPR) proteins (Kodama et al., 2010; Gardiner et al., 2011; Kodama et al., 2011). We identified 16 WPRs in *A. thaliana* and 17 WPRs in maize. A protein tree was inferred (Supplemental Figure S2), and the proteins fell into five clades: WPRA, PMI, WEB/WEL, WPRB, and WPRC. The four maize proteins interacting with PAN2 fell into the WPRA and WPRB clades; we named these proteins as

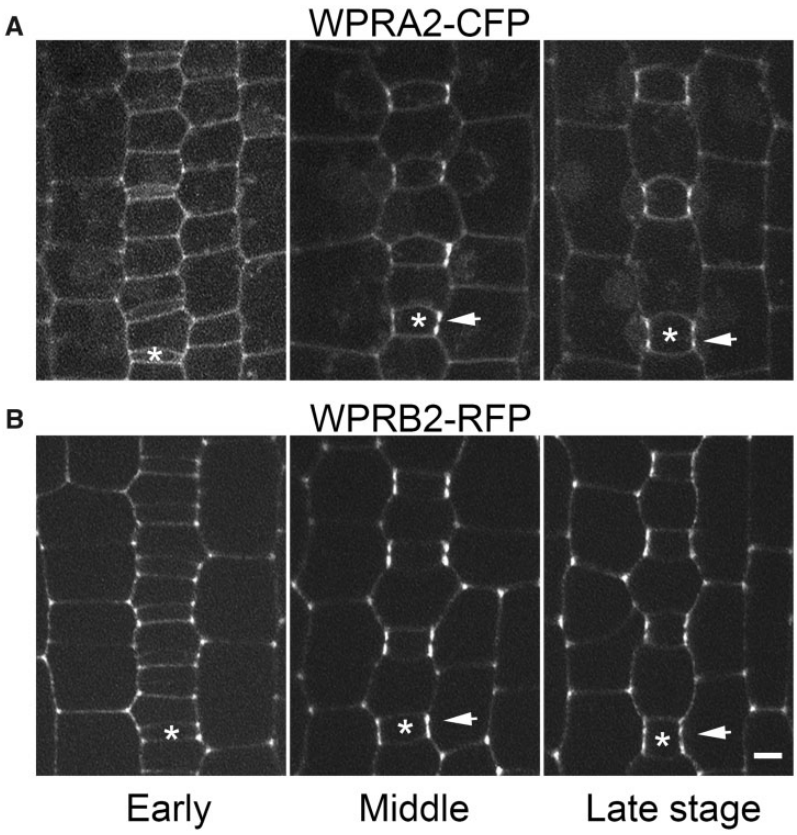

Figure 1 CFP-WPRA2 and RFP-WPRB2 polarize in developing subsidiary mother cells. The stomatal division zone of the leaf epidermis of transgenic maize plants expressing fluorescent fusion proteins was dissected and analyzed. Three different developmental stages were selected according to GMC width and SMC division status to observe the localization of CFP-WPRA2 (A) and RFP-WPRB2 (B). Arrows point to sites of CFP-WPRA2 or RFP-WPRB2 accumulation in SMCs where they contact the adjacent GMC. Asterisks mark a GMC within each stomatal row. Scale bar = 5 μm, all images scaled identically.

WPRA1, WPRA2, WPRB1, and WPRB2. WPRs have predicted coiled-coil domains in their central plant-specific DUF827 region, flanked by uncharacterized N- and C-terminal regions.

Thus far, all proteins identified in the BRK–PAN–ROP pathway polarly localize in SMCs prior to division (Cartwright et al., 2009; Humphries et al., 2011; Zhang et al., 2012; Facette et al., 2015). To determine if WPR proteins play a role in SMC polarization, we determined if they were similarly polarized. We created stable transgenic maize lines expressing either CFP-WPRA2 or RFP-WPRB2. WPRA1 and WPRA2 are 89% identical, and WPRB1 and WPRB2 are 56% identical, but WPRA2 and WPRB2 are only 28% identical. Due to the cost of maize transgenics, we chose one representative A family member and one B family member for our analyses. Genomic fragments containing the native promoter, introns and terminator were used. At early stages of stomatal development prior to the SMC formation, CFP-WPRA2 (Figure 1A) and RFP-WPRB2 (Figure 1B) predominantly localize to the cell periphery in all cell types, with low levels of cytoplasmic fluorescence. RFP-WPRB2 is enriched in cell corners, similar to BRK1–CFP (Facette et al., 2015). As development proceeds, CFP-WPRA2 and RFP-WPRB2 become enriched in the SMC at the site of GMC contact and remain polarized after SMC division (Figure 1). Plasmolysis experiments confirm that CFP-WPRA2 and RFP-WPRB2 are polarized in the SMC, not the GMC (Supplemental Figure S3). We further validated the localization by performing immunofluorescence using custom-generated antibodies that recognize either WRPA1/WPRA2 or WPRB2 (Supplemental Figure S4). Similar to the transgenic lines, we saw polarized localization in SMCs and enrichment at cell corners. Thus, the localization of WPRA2 and WPRB2 is similar to that of known BRK–PAN–ROP pathway components and supports a role in SMC polarization. Notably, WPR proteins contain no predicted transmembrane domains or lipidation signals, indicating their association with the membrane is either peripheral or via interactions with other membrane proteins.

WPRs interact with PAN1 and PAN2

To confirm the WPR–PAN2 interaction, we performed reciprocal co-IP/MS experiments using three strategies, using either our fluorescent protein fusion lines or a native antibody. First, we used anti-GFP to immunoprecipitate WPRA2 from transgenic plants expressing CFP-WPRA2; non-transgenic wild-type plants were used as a negative control. Second, we used anti-RFP to immunoprecipitate WPRB2 from transgenic plants expressing RFP-WPRB2, again using nontransgenic plants as a negative control. Third, we used

Table 1 WPR proteins interact with other WPR family members and PAN receptors

Gene ID		Gene name	Rep1 # Unique Peptides	Rep2 # Unique Peptides	Rep3 # Unique Peptides	Control 1 # Unique Peptides	Control 2 # Unique Peptides	Control 3 # Unique Peptides
Anti-GFP	Zm00001d041088	**WPRA2 (bait)**	28	42	2	2	0	0
	Zm00001d007164	WPRB2	5	3	0	0	0	0
	Zm00001d010610	WPRB3	15	13	0	0	0	1
	Zm00001d029420	WEB subfamily protein	5	7	0	0	0	0
Anti-WPRA1/A2	Zm00001d023629	**WPRA1 (bait)**	24	19	26	0	1	2
	Zm00001d041088	**WPRA2 (bait)**	26	19	27	0	0	0
	Zm00001d047516	WPRB1	5	4	6	0	0	0
	Zm00001d007164	WPRB2	19	21	21	0	0	0
	Zm00001d010610	WPRB3	24	21	24	0	1	0
	Zm00001d026139	WPRC subfamily protein	2	1	0	0	0	0
	Zm00001d000443	WPRC subfamily protein	2	2	0	0	0	1
	Zm00001d048523	WEB subfamily protein	2	2	2	0	0	0
	Zm00001d007862	PAN2	4	5	4	0	0	2
	Zm00001d031437	PAN1	2	5	2	0	0	0
Anti-RFP	Zm00001d007164	**WPRB2 (bait)**	18	20	17	0	1	0
	Zm00001d023629	WPRA1	18	16	16	0	0	0
	Zm00001d041088	WPRA2	15	21	20	0	2	0
	Zm00001d010610	WPRB3	1	2	1	0	0	0
	Zm00001d007826	PAN2	3	0	1	0	0	0

WPR-interacting proteins identified by Co-IP/MS. For a complete list of all proteins, see Supplemental Data Set 1. Three different experiments were performed. 1: Anti-GFP was used to pull down WPRA2 and interacting proteins from extracts of plants expressing CFP-WPRA2 and from non-transgenic plants as a negative control. 2: Anti-WPRA1/A2 was used to pull down WPRA1/A2 and interacting proteins from B73 extracts; negative controls used the same extracts but omitted the anti-WPRA1/A2 antibody. 3: Anti-RFP was used to pull down WPRB2 and interactors from extracts of plants expressing RFP-WPRB2 and from non-transgenic plants as a negative control. B73 vs4 gene codes are used to identify proteins, and the number of unique peptides (# peptides) is listed. The baits WPRA2, WPRA1/A2, and WPRB2 are highlighted in bold.

an antibody raised against WPRA1/A2 (see "Materials and methods"; Supplemental Figure S4) to pull down endogenous WPRA from nontransgenic plant extracts, with reactions omitting this antibody as a negative control. In each experiment, three biological replicates were performed. After comparing relative abundances of identified proteins with corresponding negative controls, we found WPRA family proteins co-precipitated with WPRB family proteins in all three assays (Table 1; Supplemental Data Set 2). Moreover, we found that both PAN1 and PAN2 co-precipitated with WPRA1/A2, and PAN2 co-precipitated with RFP-WPRB2. In addition, the enrichment of WPRB3 peptides was detected in CFP-WPRA2 and WPRA1/A2 immunoprecipitates, suggesting that WPRB3 may also associate with WPRA proteins.

To validate these interactions and test whether WPRs directly interact with PAN1 and PAN2, yeast two-hybrid (Y2H) assays were conducted using intracellular portions of PAN1 and PAN2 as bait (Zhang et al., 2012) and WPRA1, WPRA2, WPRB1, WPRB2, and WPRB3 as prey. In these assays, no interaction between WPRA1 or WPRA2 and PAN1 or PAN2 was observed. However, we found that both WPRB1 and WPRB2 interact with PAN1 and PAN2. WPRB3 interacts with PAN2 but not PAN1 (Figure 2, A and B). These data confirm a direct physical interaction between the intracellular regions of PAN and WPRB proteins. Our co-IP MS data suggest that WRPA–WPRB interact, and previous work has shown that *A. thaliana* WEB1 interacts with PMI2 and itself (Kodama et al., 2010). We performed Y2H assays to determine if maize WPR proteins also form homo/heterodimers and found several hetero- and homodimer combinations (Figure 2, C and D). Negative controls for all assays are shown in Figure 2E. This included heterodimers between WPRA and WPRB proteins. This potentially explains why the co-IP/MS data indicate that PAN proteins interact with both WPRA and WPRB proteins, yet no direct interaction between WPRA and PAN proteins was observed. Taken together, the co-IP/MS combined with Y2H assays demonstrated an interaction network (Figure 2F). We suggest that WPRB could be mediating a WPRA–WPRB heterodimer interaction with both PAN1 and PAN2 (Figure 2G).

WPR proteins act after PAN2 but before PAN1 in the BRK–PAN–ROP pathway

Grass stomatal development occurs sequentially, where cells closest to the leaf base are developmentally less advanced and cells more distal from the leaf base are more developmentally advanced. Therefore, in a single leaf, all stages of development can be observed (Supplemental Figure S1, A–F). SMCs are initially unpolarized. As development proceeds, proteins important for cell polarization become enriched at the GMC–SMC contact site, in sequence. Previous studies have demonstrated that BRK–PAN–ROP pathway components polarize sequentially in SMCs in the following order: BRK1, PAN2, PAN1, followed by the formation of a cortical F-actin patch at the GMC contact site (Cartwright et al., 2009; Zhang et al, 2012; Facette et al., 2015; Supplemental Figure S1G). To determine the relative timing of WPR protein polarization, we examined SMCs in plants co-expressing either CFP-WPRA2 or RFP-WPRB2 with BRK1–CFP, PAN2–

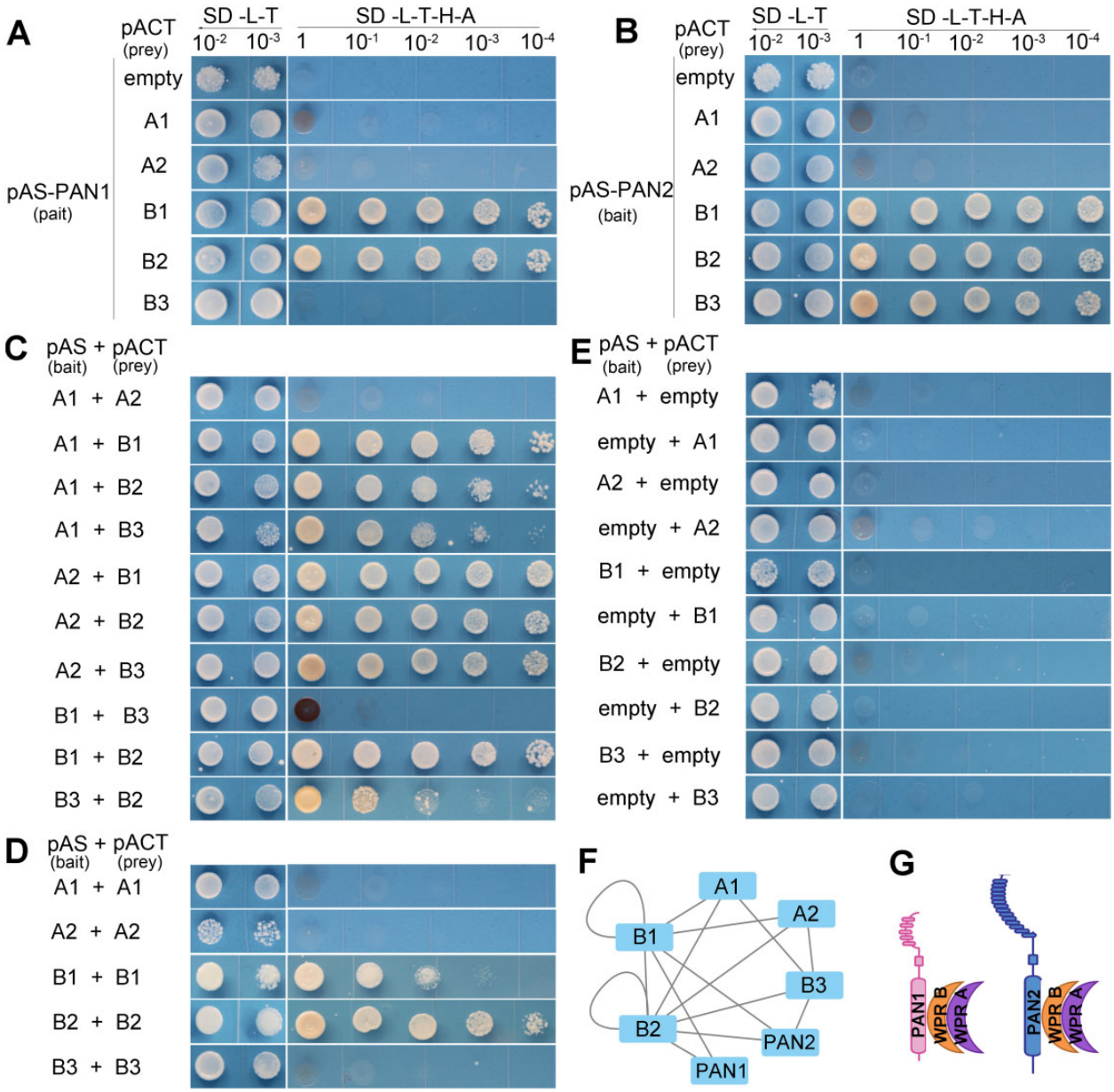

Figure 2 Y2H analysis of WPR and PAN protein interactions. Interactions were assessed using the GAL4-based Y2H system. Yeast was grown at different dilutions on nonselective (−L−T) and selective (−L−T−A−H) media. Soluble intracellular regions of PAN1 and PAN2 were used. A, B, interactions of PAN1 and PAN2 with WPRA1, WPRA2, WPRB1, WPRB2, and WPRB3. C, Heterodimer formation was assessed between WPRA1, WPRA2, WPRB1, WPRB2, and WPRB3. D, Homodimer formation was assessed between WPRA1, WPRA2, WPRB1, WPRB2, and WPRB3. E, Negative controls using empty bait plasmid pASGW-attR or prey plasmid pACTGW-attR. F, Network diagram showing the observed interactions between WPRs and PAN1/PAN2. G, A model of protein complex formation between PAN and WPR proteins.

YFP, PAN1–YFP, or the F-actin marker FABD2-YFP (Figure 3). First, we compared the relative timing of the two WPR proteins (Figure 3A). In plants co-expressing CFP-WPRA2 and RFP-WPRB2, we observed 276 polarized SMCs. In all cells, CFP-WPRA2 and RFP-WPRB2 polarized at the GMC–SMC interface at the same time. We never observed polarization of one protein without the other. This is consistent with WPRA and WPRB proteins acting as a heterodimer. Based on this observation, we infer that polarization of either WPR protein at the GMC–SMC interface is likely indicative of the other.

Next, we compared BRK1–CFP, the earliest known marker of polarity, and RFP-WPRB2. In plants co-expressing BRK1–CFP and RFP-WPRB2, we frequently saw that BRK1–CFP had become polarized while RFP-WPRB2 had not yet become polarized (94/232 cells). The arrows in Figure 3B indicate cells where BRK1 is polarized but WPRB2 is not. Reciprocally, we never saw cells in which RFP-WPRB2 was polarized and BRK1–CFP was not polarized. This indicates that BRK1–CFP polarizes prior to RFP-WPRB2 and is consistent with previous findings that BRK1 is the earliest known marker of polarity (Figure 3B). When CFP-WPRA2 was co-

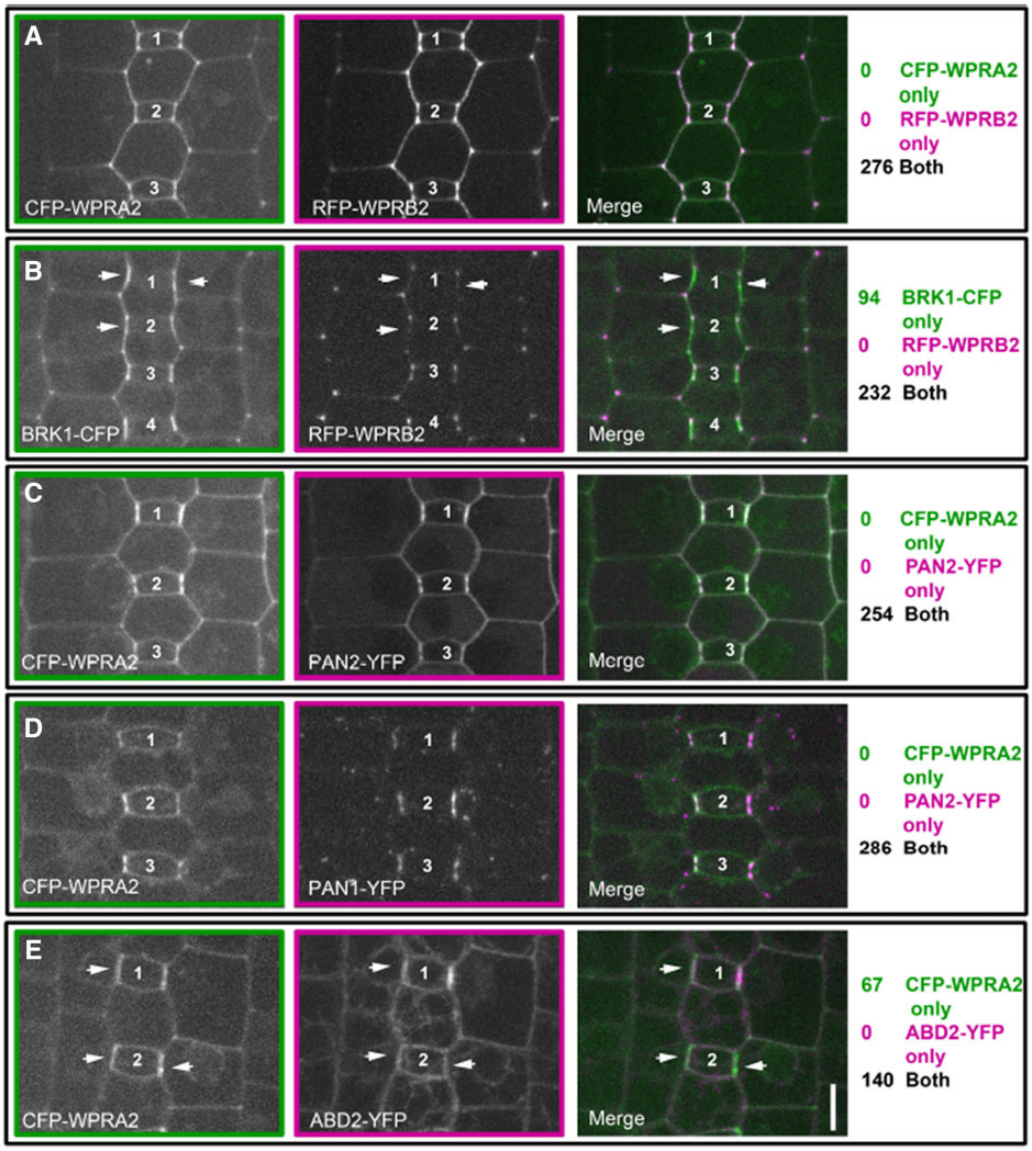

Figure 3 WPR proteins polarize in SMCs after BRK1 and before actin. The stomatal division zone of leaf 4 from plants co-expressing (A) CFP-WPRA2 and RFP-WPRB2; (B) BRK1–CFP and RFP-WPRB2; (C) CFP-WPRA2 and PAN1-YFP; (D) CFP-WPRA2 and PAN2-YFP; or (E) CFP-WPRA2 and FABD2-YFP were analyzed for enrichment at the GMC–SMC interface. Fluorescent proteins were scored as polarized when fluorescence was brighter at the SMC–GMC interface than at the cell periphery distal to the GMC. Within each panel, the same GMCs imaged in the different channels (and the subsequent merged panel) are numbered. Arrows point to SMCs where one fluorescent protein is polarized but not the other. Counts of individual SMCs that had only one fluorescent protein, or both, are listed at the right of the images. All images are at the same scale and are Z-projections of seven confocal slices. Scale bar in the merged panel of (E) is 10 μm, all images scaled identically.

expressed with either PAN2-YFP (Figure 3C) or PAN1-YFP (Figure 3D), SMCs always showed co-polarization at the GMC contact site. The relative timing of WPR proteins and PAN1 receptors cannot be resolved from co-localization; our data indicates they polarize at the same time. The accumulation of F-actin at the GMC–SMC interface is the last known marker of polarity. In SMCs co-expressing CFP-WPRA2 and FABD2-YFP, we could never see polarized accumulation of FABD2-YFP when CFP-WPRA2 was not polarized. However, we could see polarized accumulation of CFP-WRPA2 when actin had not yet accumulated in 67/140 cells (Figure 3E), suggesting that WPRA2 polarizes prior to the actin patch in developing SMCs. Thus, WPR proteins polarize after BRK1–CFP but prior to actin.

The co-expression of WPR proteins and PAN proteins indicate they polarize at (or very close to) the same time. To investigate the possible dependence of WPR polarization on the functions of known BRK–ROP–PAN pathway components, we examined the polarization of CFP-WPRA2 and RFP-WPRB2 in *brk1*, *pan1*, and *pan2* mutants (Figure 4). Homozygous mutant plants were compared to heterozygous siblings that were grown in parallel. Maize transgenics are generated in a hybrid background, and different inbred lines have a large amount of genotypic variation that may persist

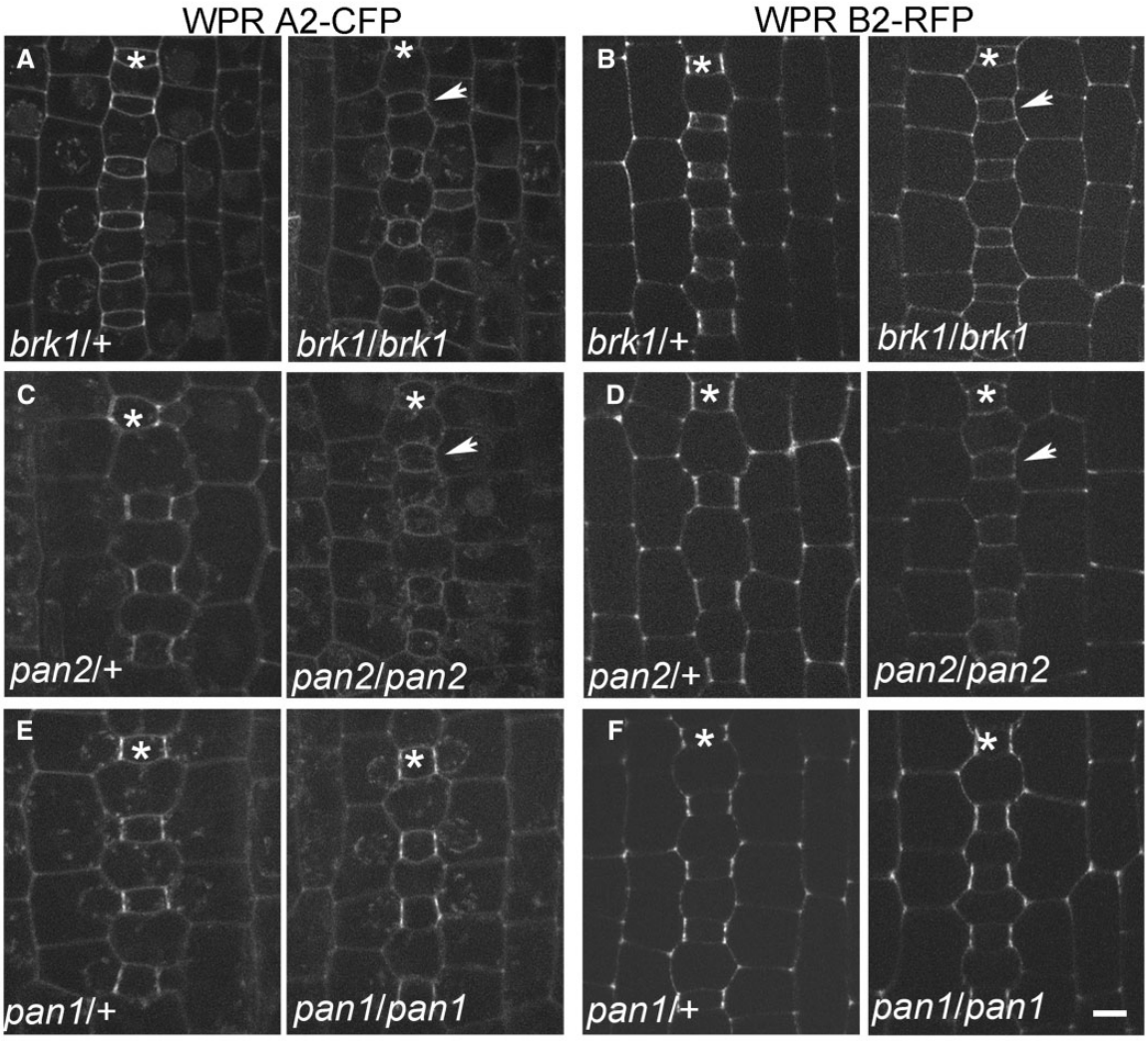

Figure 4 Polarization of WPR proteins depends on BRK1 and PAN2 but not PAN1. Localization of CFP-WPRA2 and RFP-WPRB2 in *brk1*, *pan2*, and *pan1* mutants and nonmutant siblings was analyzed in developing leaf 4. CFP-WPRA2 (A) and RFP-WPRB2 (B) in developing stomata of a *brk1* mutant and nonmutant (heterozygous) sibling. CFP-WPRA2 (C) and RFP-WPRB2 (D) in developing stomata of a *pan2* mutant and nonmutant (heterozygous) sibling. CFP-WPRA2 (E) and RFP-WPRB2 (F) in developing stomata of a *pan1* mutant and nonmutant (heterozygous) sibling. Asterisks mark GMC rows. Arrows point to SMCs without polarized localization of CFP-WPRA2 or RFP-WPRB2. Three to six plants of each genotype were used for data collection. Scale bar, 5 μm, all microscopy images scaled identically.

after backcrossing. By comparing mutants to phenotypically wild-type, heterozygous sibling plants, background genetic variation is accounted for and any unexpected silencing of the transgene is also controlled for.

Previously, it was shown that in the *brk1* mutant, PAN1 and PAN2 do not polarize (Facette et al., 2015). Similarly, PAN1 does not polarize in a PAN2 mutant (Zhang et al., 2012). In the *brk1* mutant, both CFP-WPRA2 and RFP-WPRB2 lost their polarized accumulation at the SMC–GMC interface (Figure 4, A and B). This is consistent with the co-localization data and indicates that WPRs act downstream of BRK1. Polarized localization of both CFP-WPRA2 and RFP-WPRB2 at the GMC contact site of SMCs is completely lost in the *pan2* mutant (Figure 4, C and D). In contrast, both WPR proteins remain polarized in the *pan1* mutant (Figure 4, E and F). Thus, although we observed no timing difference in the polarized accumulation of PAN2, PAN1, and WPR proteins, PAN2 acts genetically upstream of WPRs and promotes their polarized accumulation. However, PAN1, which acts downstream of PAN2, is not required for WPR polarization.

CRISPR/Cas9-mediated knockout of *Wprb1* and *Wprb2* causes subsidiary cell defects

To determine whether WPRs are required for asymmetric cell division during maize stomatal development, we used CRISPR/Cas9 to generate *wpr* mutants. The coding sequences of *Wpra1* and *Wpra2* are 92% identical; therefore, both genes were targeted using the same two guide RNAs. *Wprb1*

and *Wprb2* are 57% identical, and therefore two different guide RNAs were used in a single construct to separately target the two genes. Single mutants were identified for each gene (Supplemental Figure S5, A–C). The edited lines were backcrossed with B73 and the transgene was segregated away. Single mutants were then crossed to obtain true-breeding double mutant lines. No stomatal phenotypes were observed in single mutant plants, possibly due to redundancy. Therefore, we made double mutants with *wpra1* and *wpra2*, and with *wprb1* and *wprb2*. Despite PCR and sequence-based genotyping of many hundreds of plants from several different crosses, we never recovered *wpra1;wpra2* double homozygous mutants (Supplemental Figure S5D). This might reflect an essential shared function for the two genes in the male gametophyte, based on the high expression level of *wpra1* and *wpra2* in maize pollen (Supplemental Figure S5E). We were, however, able to generate *wprb1;wprb2* double homozygous mutants by crossing *wprb1/wprb1;wprb2/+* plants with *wprb1/+;wprb2/wprb2* plants (which generated double mutants at a higher frequency than a selfed double heterozygote). No stomatal phenotypes were observed in *wprb1* or *wprb2* single homozygotes; however, *wprb1/wprb1;wprb2/wprb2* double mutants have an increased percentage of defective subsidiary cells relative to *wprb1/+;wprb2/+*, *wprb1/wprb1;wprb2/+*, and *wprb1/+;wprb2/wprb2* siblings (Figure 5). The abnormally shaped subsidiary cells are phenotypically similar to those found in *brk1*, *pan1*, and *pan2* mutants (Supplemental Figure S1, H–K; Frank et al., 2003; Cartwright et al., 2009; Zhang et al., 2012; Facette et al., 2015). Stomatal density was unaffected in *wprb1/wprb1;wprb2/wprb2* mutants (Supplemental Figure S6). Since the aberrant subsidiary cell phenotype of *wprb1;wprb2* double mutants is mild relative to *pan1* or *pan2* mutants, we wanted to know if *wprb* mutants would enhance *pan2* phenotypes, similar to what has been observed in *rop2/4/9* mutants in combination with *pan1* (Humphries et al., 2011). However, we found that *wprb* mutations do not enhance the *pan2* phenotype (Supplemental Figure S7). We also examined *wprb1;wprb2* mutants for nuclear polarization and formation of the actin patch, two landmarks of polarity in SMCs (Supplemental Figure S8). No differences in nuclear polarization or actin patch formation were seen in *wprb1;wprb2* mutants. This may be because of the relatively mild defect or redundancy within the family. Higher order mutants, such as the closely related *wprb3* mutant, could be informative.

In addition to loss-of-function phenotypes, we examined our native promoter-fluorescent protein fusion transgenics to determine if mild overexpression, resulting from the co-expression of these FPs in a wild-type background with endogenous *Wpr* genes, would cause defective stomatal phenotypes. Plants expressing RFP-WPRB2 or CFP-WPRA2 in B73 indeed had mild subsidiary cell defects, further supporting that WPR proteins have a function in subsidiary cell division (Figure 5, E and F). These results indicate that both WPRA and WPRB family members participate in stomatal development, and suggest that WPRA1 and WPRA2 are important for the viability or function of male gametophytes.

WPRB proteins directly interact with F-actin

Since WPR proteins contain no discernable domains other than DUF827, their molecular role is unclear. We hypothesized that WPRs might interact with F-actin based on the importance of actin in SMC polarization and because Arabidopsis WEB1 and PMI2 have roles related to actin-based regulated chloroplast movement (Kodama et al., 2010). Although we did not see obvious co-localization of WPR proteins with actin filaments in maize, membrane localization has been observed for other known actin-associated proteins such as BRK1 and WAL (Facette et al., 2015; Sugiyama et al., 2019). When overexpressed in *Nicotiana benthamiana* cells, WAL localizes to actin cables (as opposed to membranes). To determine whether overexpressed WPRs similarly co-localize with F-actin in vivo, we transiently overexpressed GFP-tagged WPRA2, WPRB1, WPRB2, and WPRB3 proteins in *N. benthamiana* epidermal cells. GFP-WPRA2 localized exclusively at the cell periphery/membrane (Figure 6C). However, GFP-WPRB1 (Figure 6D), GFP-WPRB2 (Figure 6E), and GFP-WPRB3 (Figure 6F) were observed in filament-like structures and possibly also in the plasma membrane. When GFP-WPRB2 is co-expressed with Lifeact-RFP (actin filament marker), the WPRB2-labeled filamentous structures extensively overlapped with Lifeact-RFP signals, particularly in the thick actin cables (Figure 6, L–N). We treated GFP-WPRB2-expressing *N. benthamiana* leaves with Latrunculin B, an inhibitor of actin polymerization. The GFP-WPRB2 filamentous structures were disrupted but remained intact in the Dimethylsulfoxide (DMSO) control (Figure 6, O and P; Supplemental Figure S9). Thus, WPRB2 is an F-actin associated protein.

WPR proteins do not show significant sequence similarity to other known actin-associated proteins. To identify which region of the WPRB2 protein is responsible for its localization to filamentous structures, various WPRB2 fragments were used for transient *N. benthamiana* expression assays (Figure 6A). Surprisingly, the central conserved DUF827 domain is not responsible for filamentous localization. Instead, we found that the N-terminal 67 amino acids of WPRB2 is sufficient for filamentous localization in *N. benthamiana* cells (Figure 6J). Longer fragments containing the N-terminal 67 amino acids of WPRB2 were also found in filamentous structures, including GFP-WPRB2ΔC (Figure 6G) and GFP-WPRB2N142 (Figure 6K). Any construct lacking the N-terminal domain does not label actin filaments, such as GFP-WPRB2ΔN (Figure 6H) and GFP-WPR B2ΔNC (Figure 6I). We obtained similar results using full-length and truncated CFP-tagged constructs that were fused at the C-terminus (rather than at the N-terminus) of WPRB2 (Supplemental Figure S10). Conserved residues in the N-terminus of DUF827 proteins are highlighted in Supplemental Figure S11. Together, these data confirm that the N-terminal

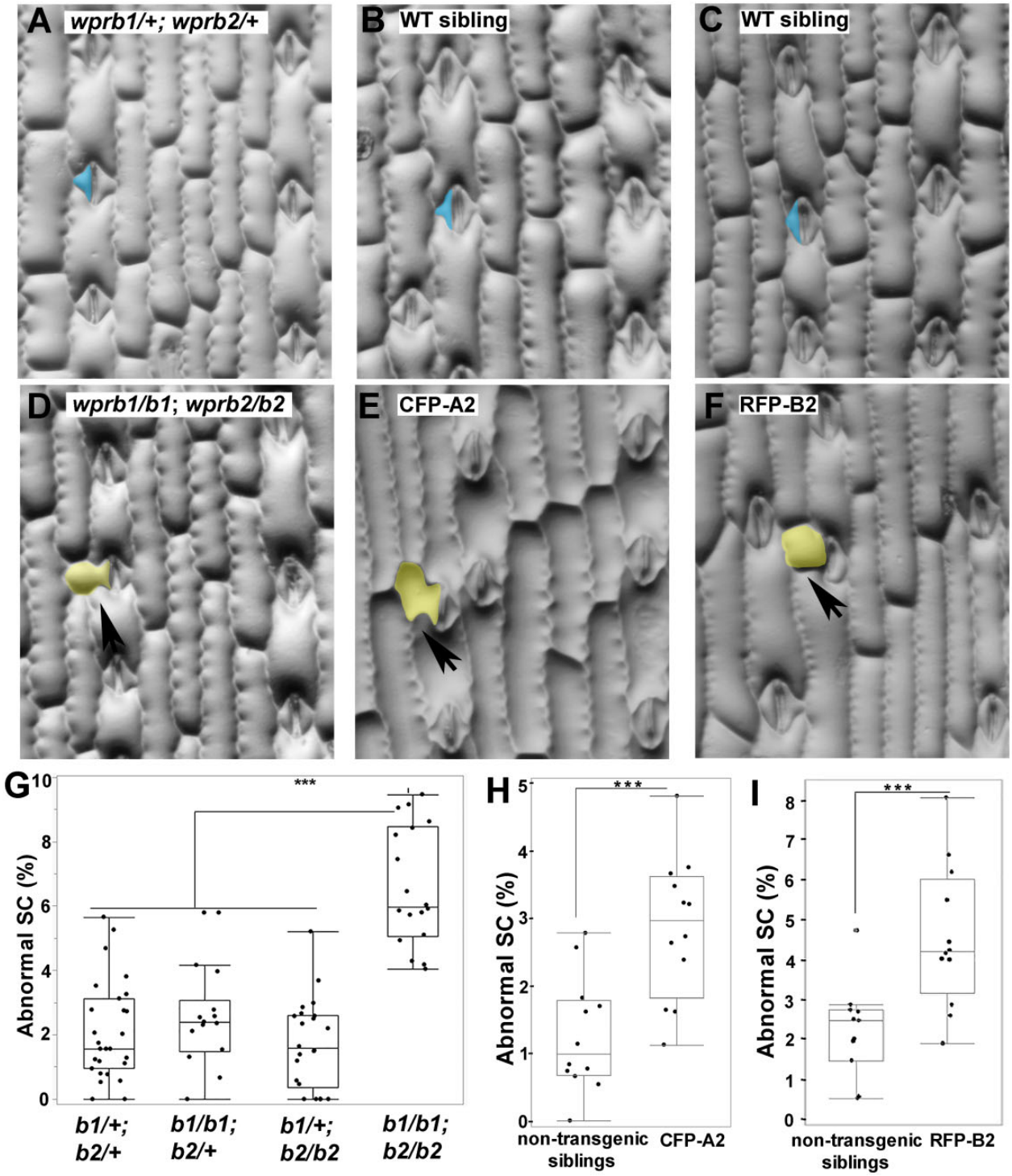

Figure 5 CRISPR–Cas9-induced *wprb1*;*wprb2* double mutants and CFP-WPRA2- and RFP-WPRB2-expressing lines have subsidiary cell defects. A–F, Representative image of the third leaf epidermis of *wprb1/+*;*wprb2/+* and *wprb1/wprb1*;*wprb2/wprb2* mutants (A and D), CFP-WPRA2 transgenic plants and nontransgenic siblings (B and E), and RFP-WPRB2 transgenic plants and nontransgenic siblings (C and F). Examples of normal subsidiary cells in (A), (B), and (D) are false-colored blue, and abnormal subsidiary cells in (D), (E), and (F) are false-colored yellow and marked with black arrows. G, Quantification of abnormal subsidiary cells in *wprb1/+*; *wprb2/+* (n = 27 plants), *wprb1/b1*;*wprb2/+* (n = 14 plants), *wprb1/+*;*wprb2/wprb2* (n = 22 plants), and *wprb1/wprb1*;*wprb2/wprb2* (n = 18 plants). For each plant, 100–200 subsidiary cells were examined. P-value from Student's t test comparing each genotype, ***$P \leqslant 0.001$. H, I, Quantification of abnormal subsidiary cells in CFP-WPRA2- or RFP-WPRB2-expressing plants and nontransgenic siblings grown in parallel (n = 11–12 plants and 120–200 cells per genotype). Box plots show median values (center line), 25th to 75th interquartile range (box) and 1.5*interquartile range (whiskers). Student's t tests were performed, ***$P \leqslant 0.001$.

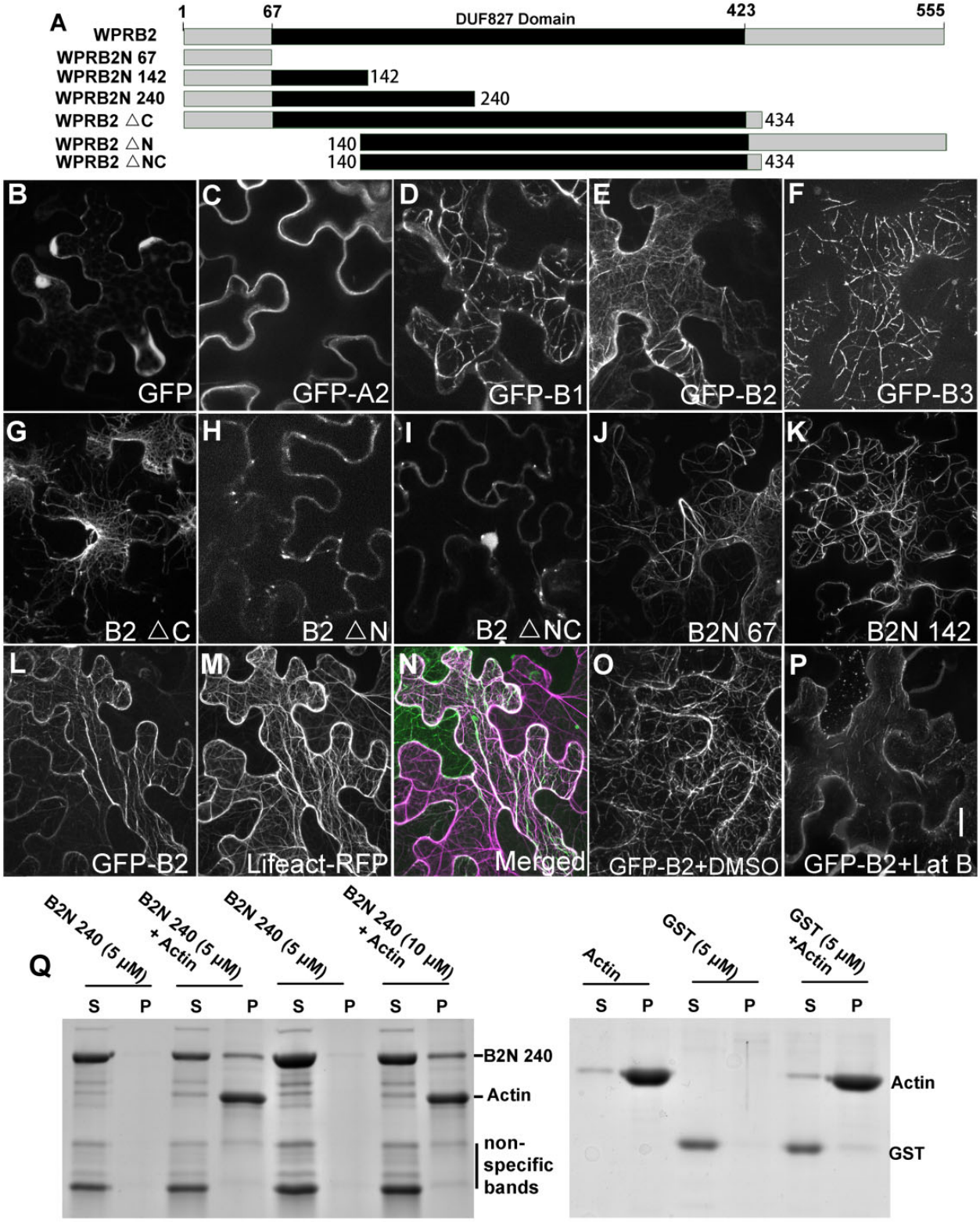

Figure 6 WPRB interacts with F-actin. A, Schematic depicting WPRB2 and truncated versions. B–F, Confocal images of transiently expressed full-length GFP fusion proteins in tobacco. Transient expression of GFP only (B), GFP-WPRA2 (C), GFP-WPRB1 (D), GFP-WPRB2 (E), or GFP-WPRB3 (F). G–K, Transient expression of truncated WPRB2 proteins fused to GFP in tobacco leaves. The co-expression of GFP-WPRB2 (L) with Lifeact-RFP labeled actin microfilaments (M); merged image (N) of the same cell. Tobacco leaves expressing GFP-WPRB2 were treated with DMSO (negative control, O) or 40-μM Latrunculin B (P) for 2 h. Scale bar in (P) = 10 μm, all images scaled identically. Q, High-speed co-sedimentation of GST-tagged WPRB2N240 with F-actin. After centrifugation at 100,000*g*, the proteins in the supernatant (S) and pellet (P) were resolved by SDS–PAGE and visualized with Coomassie Blue staining. GST protein was used as a negative control.

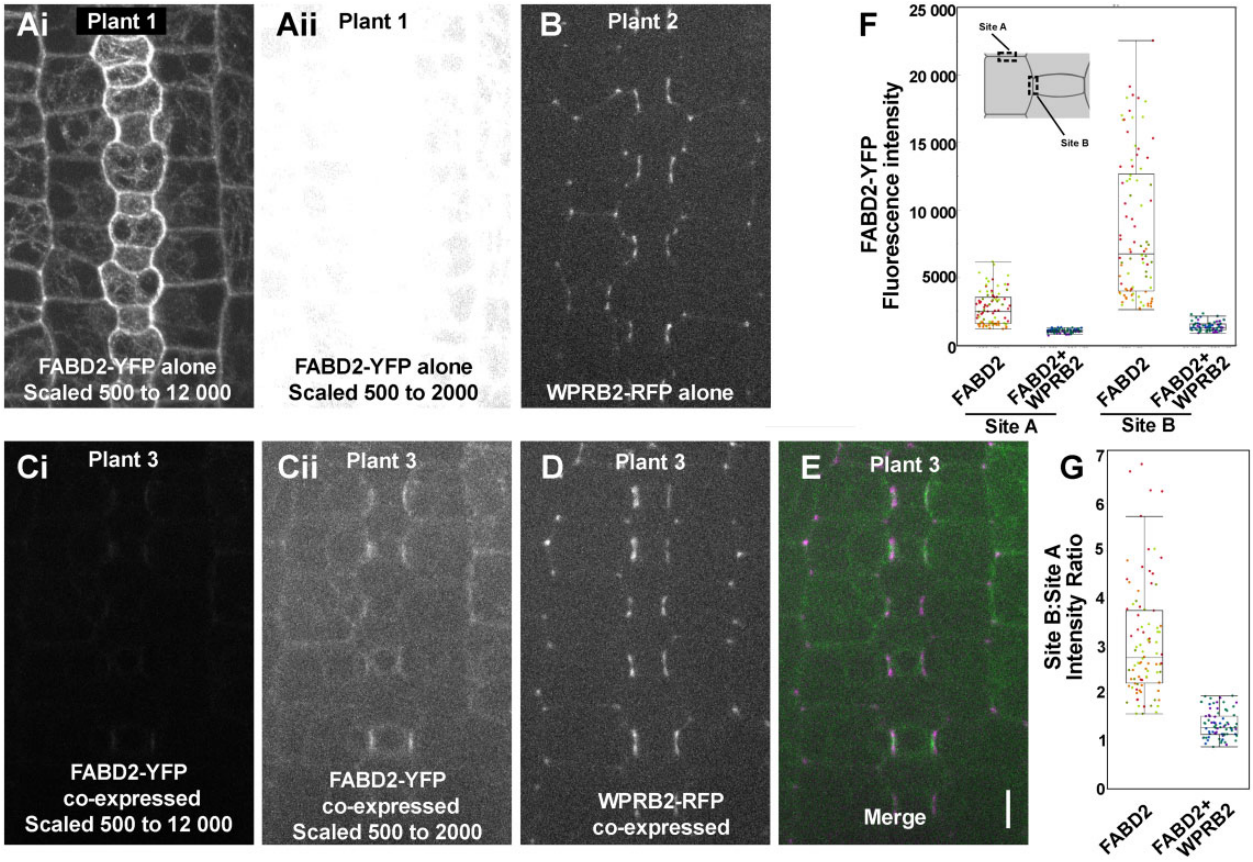

Figure 7 Fluorescence intensity of ABD2-YFP decreases in RFP-WPRB2-expressing plants. Plants expressing RFP-WPRB2 and FABD2-YFP were crossed, and the progeny independently segregated the two markers. A(i) and A(ii) Plant only expressing FABD2-YFP. An identical image is shown in A(i) and A(ii). In Ai, the 16-bit image was scaled from 600 to 12,000 prior to converting to 8 bit. A(ii) was scaled 500 to 2,000. B, Plant only expressing RFP-WPRB2. C–E, Plant co-expressing FABD2-YFP (C, green in E) with RFP-WPRB2 (D, magenta in E). C(i) and C(ii) show an identical image of the ABD2-YFP channel, where C(i) is scaled the same as A(i) and C(ii) is scaled the same as A(ii), for comparative purposes. Image intensity in (B) and (D) are scaled identically. Scale bar in *E* = 10 microns, all images are scaled identically. F, Quantification of fluorescence intensity of SMC lateral cell side (site A) and SMC–GMC interface (site B) in FABD2-YFP-only plants (n = 5 plants, 292 cells) and RFP-WPRB2- and FABD2-YFP-co-expressing plants (n = 3 plants, 164 cells). One-sided t tests indicate lower values in co-expressing plants ($P < 0.0001$). G, Ratio of intensities measured in (F). A two-sided t test indicates a significantly lower ratio in the co-expressing cells ($P < 0.0001$).

67 amino acids of WPRB2 are necessary and sufficient for its filamentous localization.

To ask whether WPRB2 directly interacts with F-actin, we performed in vitro actin co-sedimentation assays. We used the slightly larger WPRB2N240 fragment, as the smaller WPRB2N67 fragment is similar in size to actin and made interpretation of the results difficult. WPRB2N240 is soluble in the absence of F-actin but can be found in the pellet in the presence of F-actin (Figure 6Q). The amount of WPRB2N240 appearing in the pellet is concentration dependent. Together, our localization and co-sedimentation experiments suggest that WPRB2 directly binds to F-actin via its N-terminal domain.

Physical interactions of WPR proteins with both PAN receptors and the actin cytoskeleton link together previously identified components of the BRK–PAN–ROP pathway. Potentially, WPRs may regulate actin polymerization, stability, or organization during some step of SMC polarization. Future studies will help resolve the relationship between WPRB proteins and actin. Intriguingly, during co-localization experiments in stably transformed maize plants described earlier (Figure 3), we noticed that the fluorescence intensity of the actin marker FABD2-YFP was reduced in RFP-WPRB2-co-expressing plants compared with in RFP negative siblings, in all cell types. Figure 7 shows the YFP channel in a plant expressing FABD2-YFP alone [Figure 7A(i) and A(ii)], versus a sibling plant co-expressing both FABD2-YFP and WPRB2-RFP [Figure 7C(i) and C(ii)], using identical acquisition settings. Fluorescence is barely visible in the co-expressing plants when the images are scaled at a range that is appropriate for the ABD2-YFP alone plants [Figure 7A(i) versus C(i)]. Reciprocally, when the YFP channel is scaled appropriately for the co-expressing plants, the image is overexposed [Figure 7A(ii) versus C(ii)]. WPRB2-RFP intensity levels were similar in all sibling plants (Figure 7, B and D). We quantified the fluorescence in SMCs and found decreased FABD2-YFP fluorescence at the GMC contact site (Site B) as well as at the lateral side of the SMC (Site A; Figure 7F). The ratio of

intensities indicates the polarized site is more affected (Figure 7G). This could be because of a critical function of WPRB2-RFP in promoting actin accumulation at the polarized site, rendering it more sensitive. It may be that more of an effect is seen at the polarized site; however, because more WPRB2-RFP accumulates there. Immunoblotting indicates that the overall actin levels are unchanged in RFP-WPRB2-expressing cells (Supplemental Figure S12). This suggests that the observed decrease in FABD2-YFP fluorescence could have a negative effect on actin stability or alters actin in a way such that FABD2-YFP cannot bind as effectively.

Our previous data indicate that the expression of either CFP-WRPA2 or RFP-WPRB2 results in a low frequency of abnormal subsidiary cells (Figure 5), yet only WPRB (and not WPRA) proteins bind F-actin (Figure 6). We quantified whether CFP-WPRA2, like RFP-WPRB2, had an effect on FABD2-YFP intensity (Supplemental Figure S13). No similar decrease in FABD2-YFP intensity was observed in cells expressing CFP-WRPA2, consistent with the observation that only WPRB, and not WPRA, proteins bind F-actin.

Since actin is important in SMCs in early polarization, prior to WPR polarization (e.g. BRK proteins) and in late steps after WPR polarization (e.g. the formation of the actin patch), we wanted to know if polarization of WPRB2 is maintained or stabilized by actin. We treated maize leaves expressing either RFP-WPRB2 or FABD2-YFP with Latrunculin B. After 4 h, 40-µm Latrunculin B treatment led to efficient depolymerization of actin in SMCs, including the dense patches of actin at the SMC–GMC interface (Supplemental Figure S14). However, the disruption of actin does not affect the localization of RFP-WPRB2. This suggests that WPRB2 is not dependent on actin networks for maintaining its polarization. Together, these results suggest that WPRB2 interacts with actin filaments in a manner that destabilizes them, at least when present in excess of normal amounts. This offers a potential explanation for how WPRs may impact actin-dependent processes in polarizing SMCs.

Discussion

We demonstrated that WPR proteins function in the BRK–PAN–ROP pathway for subsidiary cell formation during maize stomatal development and physically interact with the receptor proteins PAN2 and PAN1. Like other proteins in the BRK–PAN–ROP pathway, WPRs polarize in SMCs at the site of GMC contact. The polarized accumulation of WPRs in SMC depends on PAN2, and genetic evidence demonstrates a function for WPRs in promoting normal SMC divisions. Like WEB1 and PMI2 in Arabidopsis, different WPR subfamily members form heterodimers, suggesting that WPR subfamily members co-operate to fulfill their function in different cellular contexts (Kodama et al., 2010).

Our analyses indicate that WPR proteins act downstream of PAN2 but upstream of PAN1, yet physically interact with both PAN1 and PAN2. This is the first observed physical link between PAN2 and PAN1, and offers a hypothesis of how PAN2 may promote polarization of PAN1, i.e. indirectly via WPR recruitment. We predict that in *wpr* mutants, PAN1 will no longer become polarized; however, gene redundancy within the WPR family makes this a nontrivial question to address. Future experiments with high-order *wpr* mutants and PAN1-YFP will further elucidate the function of WPRs in the pathway. Even though WPRA2 and WPRB2 no longer polarize in *pan2* mutants, they still localize to the plasma membrane, indicating that membrane localization is independent of PAN2.

Our data indicate that both WPRA and WPRB proteins localize predominantly to the plasma membrane and may also have cytoplasmic localization. Similar to BRK1, which is important for actin regulation, WPR proteins also localize to cell corners (Facette et al., 2015). Previous studies using transient protoplast expression of WEB1 and PMI2 indicate WEB1 localizes to the plasma membrane and can recruit PMI2 there (Kodama et al., 2010). An independent proteomic study indicated that WEB1 is predominantly localized to the cytoplasm but re-localizes to the membrane (and its phosphorylation status changes) upon blue light irradiation (Deng et al., 2014). No DUF827 family members have predicted transmembrane domains, indicating their membrane association is either peripheral or via interactions with membrane-localized proteins, or perhaps via membrane-associated actin networks. Besides WEB1 and PMI2, the other characterized DUF827 protein is TREPH1 (Wang et al., 2018). TREPH1 and maize WPRA2 are orthologs (Supplemental Figure S2). A specific residue in the C-terminus of TREPH1 is phosphorylated in response to touch, and the phenotype of the *treph1* mutant is dependent on the phosphorylation status of this residue (Wang et al., 2018). However, the same residue in maize WPRA2 is not present. If all WPR proteins are similarly phosphoregulated, this suggests that other active, as of yet undiscovered kinases may be important for WPR regulation, since both PAN1 and PAN2 are pseudokinases.

Our analysis of CRISPR–Cas9-induced mutants of WPRs demonstrated that WPRs have diverse functions in maize. We were unable to recover *wpra1*/*wpra1*;*wpra2*/*wpra2* double mutants. WPRA1 and WPRA2 are 89% similar in protein sequence and are highly expressed in pollen. CFP-WPRA2 polarly localizes to the subapex of maize pollen tubes (Supplemental Figure S5), raising the possibility that WPRA proteins play a role in pollen function. Additionally, we found that *wprb1*;*wprb2* double mutants affect subsidiary cell formation, albeit not to the same extent as *pan* mutants. This may be caused by functional redundancy with other *Wpr* genes, such as *Wprb3*.

Our discovery that WPRB proteins directly bind actin is significant as it physically links them to actin network function. WPR proteins do not share any sequence homology to known actin binding proteins; however, several DUF827 proteins were predicted, based on structural homology, to potentially bind the cytoskeleton (Gardiner et al., 2011). Surprisingly, the central conserved DUF827 domain is not the actin-binding domain. We mapped a 67-amino-acid

sequence that is necessary and sufficient for actin binding, thereby identifying a putative actin binding domain. Within this sequence, there appears to be a motif that is conserved in many but not all DUF827 proteins (Supplemental Figure S8). Even though WPRA2 also contains most of this conserved domain, we did not observe co-localization of WPRA2 to the actin cytoskeleton. This could be because the transient expression does not reflect in vivo function. Alternatively, small differences between WPRA2 and B2 sequences may account for its lack of actin binding (e.g. one of a pair of glycines conserved in many WPR proteins is aspartate in WPRA2). Further refining the region of interaction, and determining if other DUF827 proteins bind actin, would inform their function.

The significance of WPR interaction with the actin cytoskeleton is unknown and is complicated by the fact that there are several actin-related processes that occur during SMC polarization. The most plausible are: a function related to the SCAR/WAVE complex that includes BRK1, which polarizes and functions very early to promote SMC polarization; a role in localization of polarity determinants (such as vesicle trafficking); a role related to actin patch formation or function; or a role related to actin-based nuclear migration. These possibilities are not mutually exclusive. Actin filaments can facilitate polarized protein localization. For example, polarization of PIN requires an intact actin cytoskeleton (Kleine-Vehn et al., 2008). It is plausible that actin networks are responsible for the polarization of PAN1 and/or PAN2, or even the WPR proteins themselves. This function would be distinct from that of the actin patch, which appears long after PAN2, PAN1, or WPR proteins polarize. When actin patches were disrupted with Latrunculin B, this did not result in the loss of already polarized RFP-WPRB2 in maize leaves, suggesting that the actin patch does not influence WPR protein localization (and possibly function). A clue to what WPR proteins could be doing in vivo can be inferred from our observation that RFP-WPRB2 transgenic plants displayed less FABD2-YFP fluorescence than controls. This suggests that WPRB2 negatively affects the stability of actin filaments and might promote F-actin depolymerization. Alternatively, WPRB proteins could compete with ABD2 for binding sites on the F-actin polymer or somehow modify F-actin such that ABD2 does not bind as effectively. Future in vitro and in vivo work characterizing the molecular role of WPR proteins on actin dynamics, including the nucleation, severing, and bundling activities, will help determine the function of this gene family—not only in cell polarization but also during mechanosensing (i.e. TREPH1 function) or organelle movements (i.e. WEB1 and PMI2 function).

Materials and methods

Plant materials and plant growth condition

Maize (*Zea mays*) BRK1–CFP, PAN2-YFP, PAN1-YFP, and YFP-ABD2-YFP stable transgenic lines, and *brk1*, *pan1*, and *pan2* mutants were described previously (Cartwright et al., 2009, Zhang et al., 2012; Facette et al., 2015). Plants used for analysis were grown for 10–14 days in a greenhouse maintained between 20°C and 29°C. Plants were grown in Promix Professional soil supplemented with Peters Excel 15-5-15 CalMag fertilizer and chelated liquid iron (Southern Ag). Supplemental LED lights (Fluence VYPR series) were used to maintain a 16-h day length.

Generation of transgenic maize lines

Transgenic lines expressing CFP-WPRA2 or RFP-WPRB2 were created using a genomic construct. Primers are listed in Supplemental Table S1. An approximately 3-kb sequence upstream of the start codon (promoter and 5′-UTR) was amplified from B73 genomic DNA with primers WPRA2-F and WPRA2-P2 or WPRB2-F and WPRB2-P2. Genomic DNA, including all exons and introns 1 kb after the stop codon (3′-UTR), was amplified from B73 genomic DNA using primers WPRA2-P3 and WPRA2-R or WPRB2-P3 and WPRB2-R. The fluorescent protein variants Cerulean (CFP) or TagRFP (RFP) were amplified with primer Tag linker-F and Tag linker-R as described previously (Mohanty et al., 2009). N-terminal fluorescent protein fusions were assembled through fusion PCR and cloned into pDONR221. Gateway LR reactions (Thermo Fisher) were used to recombine the assembled fusion protein into the binary vector pAM1006 (Mohanty et al., 2009). The constructions were verified and introduced into Hi-II maize via *Agrobacterium tumefaciens*-mediated transformation at the Wisconsin Crop Innovation Center plant transformation facility. Primary transformants were crossed to B73 to produce T1 progeny used for immunoprecipitation experiments, and T1s were crossed with BRK1–CFP, PAN2-YFP, PAN1-YFP, and YFP-ABD2-YFP to produce T2 progeny used for imaging experiments. Primary transformants were also crossed to *brk1*, *pan1*, and *pan2* mutants, and the T1 progeny backcrossed again to mutants, to produce homozygous *brk1*, *pan1*, and *pan2* mutants expressing CFP-WPRA2 and RFP-WPRB2. In all cases, sibling plants grown simultaneously were used as controls.

Yeast Two-hybrid analysis

The GAL4-based yeast two-hybrid interaction system was used for interaction assays. The cDNA fragments encoding intracellular portions of PAN1 and PAN2 were cloned into pASGW-attR plasmid as a bait via Gateway cloning as described previously (Zhang et al., 2012). cDNA was prepared from the maize leaf stomatal division zone. Full-length cDNAs of *Wpra1*, *Wpra2*, *Wprb1*, *Wprb2*, and *Wprb3* cDNA were amplified from a maize leaf division zone cDNA preparation with primers WPRA1topo1-F + WPRA1topo-R (*Wpra1*), WPRA2topo1-F + WPRA2topo-R (*Wpra2*), WPRB1topo1-F + WPRB1topo-R (*Wprb1*), and WPRB2topo1-F + WPRB2topo-R (*Wprb2*) (Supplemental Table S1). These fragments were cloned into the entry vector pENTR/D-TOPO (Invitrogen) and further transferred destination vectors pASGW-attR (bait) and pACTGW-attR (prey; Nakayama et al., 2002). Bait and prey plasmids were co-transformed into the AH109 yeast strain. Yeast was grown on medium selecting for diploid cells (SD–

Leu–Trp) or detecting interactions (SD–Leu–Trp–Ade–His) for 2 days at 30°C.

Confocal microscopy

Plant tissues were observed using a custom-built spinning disc confocal unit (3i) equipped with an inverted fluorescence microscope (IX83-ZDC, Olympus) CSU-W1 spinning disc with 50-µm pinholes (Yokogawa), a Mesa Illumination Enhancement 7 Field Flattening unit (3i), an Andor iXon Life 888 EMCCD camera and a UPLANSAPO ×60 Silicone Oil-immersion objective (NA = 1.20, Olympus), and four laser stack with TTL controller (3i). For CFP, YFP, and RFP imaging of transgenic maize plants, a 445/515/561 dichroic (Chroma) was used. All emission filters are from Semrock. A 445-nm laser line and 483/45 emission filter (CFP), 514-nm laser and 542/27 emission filter (YFP) or 568-nm laser and 618/50 emission filter (RFP) were used. For dual imaging of GFP and RFP (*N. benthamiana* expression) a 405/488/561/640 dichroic (Chroma) was used with a 488-nm laser and 525/30 emission filter (GFP) and/or 568-nm laser with a 618/50 emission filter. Image processing was performed using Image Fiji and Adobe Photoshop version 8.0 using only linear adjustments and preserving hard edges.

Quantification of ABD2-YFP fluorescence intensity was performed using FIJI. Max projections of seven slices of 16-bit images taken on the same day with the same acquisition settings were used. Sibling plants were used as controls.

Transient expression in *N. benthamiana*

To generate 35S-expressed N-terminal GFP-tagged constructs (and truncated derivatives) and C-terminal CFP-tagged constructs (and truncated derivatives) for transient *N. benthamiana* expression, coding sequences were PCR-amplified from maize leaf cDNA with the appropriate primers (Supplemental Table S1) and cloned into the pENTR/D-TOPO entry vector (Thermo Scientific). Clones were recombined with the vectors pSITE-2CA and pSITE-1NB using LR Clonase Mix II (Thermo Scientific) to form N-terminal GFP or C-terminal CFP (Romit Chakrabarty, 2006).

For transient expression in *N. benthamiana*, *Agrobacterium* strain GV3101 harboring different constructs were resuspended in infiltration buffer (10-mM MES (pH 5.7), 10-mM $MgCl_2$, 50-mg·L^{-1} acetosyringone) and the OD_{600} was adjusted to 1.0. Equal volumes of cultures containing different constructs were mixed for co-infiltration. The resulting cultures were infiltrated into leaves of 3- to 4-week-old N. *benthamiana* plants. Leaf samples were harvested 48 h after infiltration.

Generation and purification of WPRA1/A2 and WPRB2-specific antibody

Peptides corresponding to amino acids 267–288 of maize WPRA1 and WPRA2 (LRNDFDPAAYDSLKEKLEQTNS), and amino acids 446–465 of WPRB2 (HPAPRSRDSQNMDI VGVSKGC) were synthesized, conjugated to KLH, co-injected into rabbits, and used for polyclonal antibody production in rabbits by Pacific Immunology. The resulting sera was affinity purified against the corresponding peptide using columns provided by Pacific Immunology. Affinity purified antibodies were eluted using Gentle Ag/Ab buffer (Pierce), desalted against TBS Buffer, and concentrated to 1 mg·mL^{-1} using a 30K MWCO concentrator (Pierce).

Maize division zone membrane protein extraction, immunoblotting, and co-IP/MS analysis

Protein extraction for immunoblotting of WPR proteins and co-Ips were performed as described previously (Facette et al., 2015). Briefly, 10- to 14-day-old plants were used to isolate the basal 0.5–2.5 cm of unexpanded leaves 4–6; the leaf bases were ground in liquid nitrogen. Membrane fractions of extracts from these tissues were prepared. For immunoblotting, ∼0.5 g (3–5 plants) of tissue was used and, for mass spectrometry, 1.5 g (8–10 plants) was used. Ground tissue was mixed with extraction buffer (50-mM Tris [pH 7.5], 150-mM NaCl, 5-mM EGTA, 5-mM EDTA, 0.3% β-mercaptoethanol, 1% Sigma Plant Protease Inhibitor) at a ratio of 1-mL extraction buffer for every 0.25 g of tissue. The mixture was homogenized for 10 s using an Omnitip homogenizer on ice. All subsequent steps were conducted at 4°C. The mixture was centrifuged twice at 13,000*g*. The supernatant was pelleted at 110,000*g* for 45 min. Solubilization buffer (50-mM Tris [pH 7.5], 150-mM NaCl, 1% NP-40, 10% glycerol, 0.05% sodium deoxycholate) was then added to the pellet, sonicated three times for 15 s each time, and left rotating for 1 h. For immunoblotting, extracts from B73 plants and corresponding mutants were separated via sodium dodecyl sulfate–polyacrylamide gel electrophoresis (SDS–PAGE) and analyzed using anti-WPRA1/A2 at 1 µg·mL^{-1}.

For immunoblots to detect actin in B73 and RFP-WPRB2 transgenic plants, the basal 0.5–2.5 cm of unexpanded leaves 4–6 from 14-day-old plant were ground in liquid nitrogen. Ground tissue was mixed with 500-µL extraction buffer (50-mM Tris [pH 7.5], 150-mM NaCl, 5-mM EGTA, 5-mM EDTA, 0.3% β-mercaptoethanol, 1% Sigma Plant Protease Inhibitor) and homogenized immediately using an Omnitip homogenizer for 10 s on ice. Then, the mixture was centrifuged at 15,000*g* for 10 min at 4°C.

Supernatant (protein extract) was transferred to a new tube and kept on ice for immediate use. Extracted protein (100 ng) for each plant was separated via SDS–PAGE and analyzed using anti-actin (Sigma A0480, MFCD00145889) at 1:1,000.

Co-IP/MS experiments were performed using the solubilized membrane proteins. Immunoprecipitation of PAN2-YFP was performed as in Facette et al. (2015) using anti-GFP beads (Miltenyi). PAN2-YFP immunoprecipitations and subsequent mass spectrometry runs were performed in parallel with B73 (control), BRK1–CFP, PAN1-YFP, PDI-YFP, PIN1-YFP, and RAB11D-YFP using anti-GFP beads (Miltenyi). Note that these co-IPs, except PAN2-YFP and PAN1-YFP, were presented previously in Facette et al. (2015). A WD-score (Sowa et al., 2009) was calculated to determine high

confidence interactors. Tryptic digestion and mass spectrometry was performed using a Q-Exactive mass spectrometer (Thermo Scientific, San Jose, CA, USA) as described (Facette et al., 2015).

Anti-WPRA1/A2 and anti-RFP (Rabbit polyclonal, Invitrogen R10367, Lot 2127438) were coupled with Dynabeads prepared according to the Dynabeads kit instructions (Thermo Fisher). The coupled WPRA1/A2 antibody–beads complex was added to the membrane protein extracts from B73 plants; uncoupled beads were used as a negative control. Anti-RFP coupled beads were added to the membrane protein extracts from RFP-WPRB2 transgenic plants and B73 plants as a negative control. All these samples were incubated rotating at room temperature for 30 min. Then, the Dynabeads–Co-IP complex was washed according to the Dynabeads kit instructions. After washing, the Dynabeads–Co-IP complex was digested with trypsin and run with the mass spectrometer.

For co-IP using anti-GFP to pull down WPRA2, anti-GFP beads (Miltenyi) were added to the extracts from CFP-WPRA2 transgenic plants and B73 plants (negative control), then the extracts were rotated for an additional 30 min. Miltenyi μ columns were equilibrated using a solubilization buffer as described by the manufacturer's instructions. The extracts were applied to the columns and the columns were washed and eluted following the Miltenyi μ column kit instructions. The eluted samples were digested with trypsin and run on the mass spectrometer.

For all WPR immunoprecipitations, peptides were separated by reverse-phase chromatography using nano-flow EASY-nLC 1000 UHPLC coupled to an Orbitrap Fusion mass spectrometer (Thermo Scientific) with a PepMap RSLCnano column (75 μm ID, 15 cm). Peptides were eluted over a 90-min 5%–35% ACN gradient at 300 $nL \cdot min^{-1}$. Survey scans were measured in the Orbitrap analyzer at 60,000 resolution. Data-dependent MS/MS data were collected in the linear ion trap using a 2-s cycle time with a full MS mass range from 400 to 1,800 *m*/z. Peptides (charge state 2–6) were fragmented using higher energy collisional dissociation using a normalized collision energy setting of 27. A dynamic exclusion time of 5 s was used, and the peptide match setting was enabled. RAW files were analyzed in Proteome Discoverer 2.4 (Thermo Scientific) using the SEQUEST search algorithm using version 4 of the maize genome (B73 RefGen_v4). The search parameters used were as follows: 10 ppm precursor ion tolerance and 0.4 Da fragment ion tolerance; up to two missed cleavages were allowed; dynamic modifications of methionine oxidation and N-terminal acetylation. Peptide matches were filtered to a protein false discovery rate of 5% using the Percolator algorithm. Peptides were assembled into proteins using maximum parsimony, and only unique and razor peptides were retained for subsequent analysis.

Genomic editing of maize WPRs by CRISPR–Cas9

A dual gRNA maize CRISPR/Cas9 system was used to generate *Wpr* mutants (Char et al., 2017). Transgenic Hi-II maize plants were generated at the Iowa State Plant Transformation facility, expressing Cas9 from *Streptococcus pyogenes* under the maize UBI1 promotor and two guide RNAs under the rice U6.1 and U6.2 promotor, respectively. To create *wpra1* and *wpra2* mutants, two tandem gRNAs, gRNA1: GAAACATCTTTGGATATG and gRNA2: GTGCAAG CACACGAAGAAG, were used to target identical sequences within *Wpra1* and *Wpra2*. To create *wprb1* and *wprb2* mutants, guide RNAs targeting *Wprb1* using gRNA1: GCTACATGTGATCTGGCTG or *Wprb2* using gRNA2: GCCT CCGTCGAGTCGCTG were used. Genomic edits were verified by Sanger sequencing of the target regions. Plants harboring edits were crossed to B73. Edited plants that no longer contain the transgene were confirmed and used for further analyses.

Phalloidin staining

Phalloidin staining in maize leaves was performed as previously described (Cartwright et al., 2009, Nan et al., 2019). The basal 0.5–2.5 cm of leaf 4 from *wprb1/+;wprb2/+* and *wprb1/b1;wprb2/b2* mutants was fixed and stained with Alexa fluor 488-phalloidin (Thermo Fisher). Nuclei and cell walls were stained using 10 $\mu g \cdot mL^{-1}$ propidium iodide (Thermo Fisher). Samples were mounted in ProLong Gold Antifade (Thermo Fisher). Immunolocalization of WPRA2 and WPRB2 were performed in leaf tissue excised from the basal 1 to 3 cm of unexpanded leaves of 2-week-old plants as described previously (Cartwright et al., 2009, Nan et al., 2019) using affinity-purified anti-WPRA1/A2 or WPRB2 at 2 $\mu g \cdot mL^{-1}$. Alexa Flour 488-conjugated anti-rabbit (Invitrogen) was used at a dilution of 1:500. Nuclei were stained with 10 $\mu g \cdot mL^{-1}$ propidium iodide (Sigma-Aldrich) prior to mounting in ProLong Gold Antifade (Thermo Fisher) for confocal microscopy.

Immunofluorescent detection of WPR proteins

Immunolocalization of WPRA2 and WPRB2 were performed in leaf tissue excised from the basal 1–3 cm of unexpanded leaves of 2-week-old plants as described previously (Cartwright et al., 2009, Nan et al., 2019) using affinity-purified anti-WPRA1/A2 or WPRB2 at 2 $\mu g \cdot mL^{-1}$. Secondary Alexa Flour 488-conjugated anti-rabbit (Invitrogen) was used at a dilution of 1:500. Nuclei were stained with 10 $\mu g \cdot mL^{-1}$ propidium iodide (Sigma-Aldrich) prior to mounting in ProLong Gold Antifade (Thermo Fisher).

Bacterial expression of WPR proteins

The DNA sequence of WPRB2N (1–240), which was used in the actin co-sedimentation assay, was amplified by PCR using the primers listed in Supplemental Table S1 and cloned into pGEX4T-1. Fragments of WPRA1 (63–503), WPRA2 (63–570), WPRB1 (73–421), and WPRB2 (78–429), which were used to confirm the specificity of the WPRA1/WPRA2 antibody, were also amplified by PCR using the primers listed in Supplemental Table S1 and cloned into pGEX4T-1 (Novagen) using BamHI/EcoRI sites to N-terminal glutathione S-transferase (GST) tag fusions. These constructions

were transformed into *Escherichia coli* BL21 host strains (Novagen). GST fused proteins were induced with 0.5-mM isopropyl β-D-1-thiogalactopyranoside for 20 h at 28°C. Affinity purification using a glutathione-Sepharose 4B column (GE Healthcare) was carried out as described (Harper and Speicher, 2011).

F-Actin co-sedimentation assay

WPRB2N240 was dialyzed overnight against buffer A3 (10-mM Tris–HCl, 0.2-mM $CaCl_2$, 0.2-mM ATP, and 0.5-mM DTT, pH = 7.0) . Prior to use, the protein was further purified by centrifugation at 100,000*g* for 1 h at 4°C and only soluble protein was used for the assay. A high-speed co-sedimentation assay was performed as described previously (Xiang et al., 2007). Briefly, 5-μM and 10-μM WPRB2N240 alone or mixed with 4-μM preformed F-actin was incubated in 200 μL of buffer A3 for 1 h at 25°C. The samples were centrifuged at 100,000*g* for 1 h at 4°C. GST protein was used as a negative control. The supernatants and pellets were separated and subjected to SDS–PAGE and visualized by Coomassie Blue staining.

Latrunculin B treatment

To transiently depolymerize actin microfilaments in maize leaves, leaf 4 of 2-week-old plants was excised and the basal 1–3 cm part was immersed in 40-μM Lat B (20-mM stock in DMSO) for 4 h at room temperature. To examine the LatB effect on the localization of GFP-WPRB2 in *N. benthamiana* leaves, the GFP-expressing *N. benthamiana* leaves were cut into 0.5 cm × 0.5 cm pieces and covered with 40-μM LatB for 2 h at room temperature.

Protein tree construction

Amino acid sequences of maize WPR homologs were identified using pBLAST against maize genomes. The protein tree was constructed in Molecular Evolutionary Genetics Analysis 5 (MEGA 5) software (Tamura et al., 2011) with the following parameters: multiple amino acids sequence alignment with ClustalW (Larkin et al., 2007), phylogenetic construction with the maximum likelihood method, and bootstrap tests of 1,000 replicates. WPR sequences used for the phylogenetic analysis are provided in Supplemental File S1.

Statistical tests

T tests and one-way ANOVAs were performed in JMP (SAS). Chi-squared tests were performed using an online calculator released by GraphPad Prism (https://www.graphpad.com/quickcalcs/chisquared1/) with expected values calculated by hand. Statistical output results from ANOVA, *t* tests and Chi-squared tests can be found in Supplemental Tables S2–S14.

Accession numbers

Gene and protein sequences can be found at MaizeGDB www.maizegdb.org. Accession numbers for Version 4.0/Version 5.0 of the B73 genome are: *Wpra1:* Zm00001d023629/Zm00001eb408590; *Wpra2*: Zm00001d041088/Zm00001eb133280; *Wprb1:* Zm00001d0475516/Zm00001eb395070; *Wprb2:* Zm00001d007164/Zm00001eb111490; *Wprb3:* and Zm00001d010610/Zm00001eb351980; *Brk1:* no v4.0/Zm00001eb259430; *Pan2:* Zm00001d007862/Zm00001eb117610; *Pan1*: Zm00001d031437/Zm00001eb034900.

Supplemental data

The following materials are available in the online version of this article.

Supplemental Figure S1. Progression of maize stomatal development in leaves.

Supplemental Figure S2. Protein tree of the WPR family in plants.

Supplemental Figure S3. Plasmolysis assays of CFP-WPRA2 and RFP-WPRB2 transgenic plants.

Supplemental Figure S4. Immunolocalization using validated WPRA1/2 and WPRB2 antibodies and their validation

Supplemental Figure S5. CRISPR–Cas9-induced *wpra1 and wpra2* mutants might have transmission defects.

Supplemental Figure S6. CRISPR-Cas9-induced *wprb1;wprb2* double mutants have no effect on stomatal density.

Supplemental Figure S7. Mutations in *wprb1* and *wprb2* do not enhance *pan2*/*pan2* phenotype.

Supplemental Figure S8. CRISPR–Cas9-induced *wprb1;wprb2* double mutants have no effect on polarized actin accumulation or nuclear polarization during maize SMC development.

Supplemental Figure S9. Latrunculin B-treated *N. benthamiana* leaf cells transiently expressing GFP-WPRB2 and Lifeact-RFP.

Supplemental Figure S10. Transient expression of WPRB2-CFP and its truncated proteins in *N. benthamiana* leaves.

Supplemental Figure S11. Alignment of the actin-binding domain of the WPR protein family.

Supplemental Figure S12. RFP-WPRB2 expression has no effect on the total amount of actin.

Supplemental Figure S13. Co-expression of CFP-WPRA2 with ABD2-YFP does not decrease FABD2-YFP intensity.

Supplemental Figure S14. F-actin disruption does not affect the polarized localization of RFP-WPRB2 in SMCs.

Supplemental Table S1. Primer sequences used in this study.

Supplemental Tables S2–S14. Statistical information.

Supplemental Data Set 1. Co-IP/MS results using an anti-GFP antibody and membrane extracts from PAN2-YFP, PAN1-YFP, BRK1–CFP, PDI-YFP, PIN1-YFP, Rab11D-YFP, and B73.

Supplemental Data Set 2. Co-IP/MS results using WPRA1/2, WPRA2-CFP, WPRB2-RFP as bait (and corresponding controls).

Supplemental File S1. Amino acid sequences of WPRs used for the phylogenetic analysis in Supplemental Figure S2.

Acknowledgments

We thank Steve Eyles at the UMass Institute of Applied Life Sciences Mass Spectrometry Facility, RRID:SCR_019063. We thank Chris Phillips, Bob Skalbite, Neal Woodward, and other greenhouse and farm staff at the University of Massachusetts Amherst for essential help.

Funding

This work was supported by a grant from National Science Foundation (IOS-1754665) to M.R.F. and National Institute of Health (DP2-GM119132) to E.J.B.

Conflict of interest statement. None declared.

References

Apostolakos P, Livanos P, Giannoutsou E, Panteris E, Galatis B (2018) The intracellular and intercellular cross-talk during subsidiary cell formation in Zea mays: existing and novel components orchestrating cell polarization and asymmetric division. Ann Bot **122**: 679–696

Ashraf MA, Facette M (2020) Plant biology: BASL gives the plant nucleus a sense of direction. Curr Biol **30**: R1375–R1377

Campos R, Goff J, Rodriguez-Furlan C, Van Norman JM (2020) The Arabidopsis receptor kinase IRK is polarized and represses specific cell divisions in roots. Dev Cell **52**: 183–195

Cartwright HN, Humphries JA, Smith LG (2009) PAN1: a receptor-like protein that promotes polarization of an asymmetric cell division in maize. Science **323**: 649–651

Char SN, Neelakandan AK, Nahampun H, Frame B, Main M, Spalding MH, Becraft PW, Meyers BC, Walbot V, Wang K, et al. (2017) An Agrobacterium-delivered CRISPR/Cas9 system for high-frequency targeted mutagenesis in maize. Plant Biotechnol J **15**: 257–268

Cho SO, Wick SM (1990) Distribution and function of actin in the developing stomatal complex of winter rye (Secale cereale cv. Puma). Protoplasma **157**: 154–164

Deng Z, Oses-Prieto JA, Kutschera U, Tseng TS, Hao L, Burlingame AL, Wang ZY, Briggs WR (2014) Blue light-induced proteomic changes in etiolated Arabidopsis seedlings. J Proteome Res **13**: 2524–2533

De Smet I, Beeckman T (2011) Asymmetric cell division in land plants and algae: the driving force for differentiation. Nat Rev Mol Cell Biol **12**: 177–188

Dong J, MacAlister CA, Bergmann DC (2009) BASL controls asymmetric cell division in Arabidopsis. Cell **137**: 1320–1330

Facette MR, Smith LG (2012) Division polarity in developing stomata. Curr Plant Biol **15**: 585–592

Facette MR, Park Y, Sutimantanapi D, Luo A, Cartwright H, Yang B, Bennett EJ, Sylvester AW, Smith LG (2015) The SCAR/WAVE complex polarizes PAN receptors and promotes division asymmetry in maize. Nat Plants **1**: 14024.

Facette MR, Rasmussen CG, Van Norman JM (2019) A plane choice: coordinating timing and orientation of cell division during plant development. Curr Plant Biol **47**: 47–55

Frank MJ, Smith LG (2002) A small, novel protein highly conserved in plants and animals promotes the polarized growth and division of maize leaf epidermal cells. Curr Boil **12**: 849–853

Frank MJ, Cartwright HN, Smith LG (2003) Three Brick genes have distinct functions in a common pathway promoting polarized cell division and cell morphogenesis in the maize leaf epidermis. Development **130**: 753–762

Galatis B, Apostolakos P (2004) The role of the cytoskeleton in the morphogenesis and function of stomatal complexes. New Phytol **161**: 613–639

Gardiner J, Overall R, Marc J (2011) Putative Arabidopsis homologues of metazoan coiled-coil cytoskeletal proteins. Cell Biol Int **35**: 767–774

Gray A, Liu L, Facette M (2020) Flanking support: how subsidiary cells contribute to stomatal form and function. Front Plant Sci **11**: 881

Hadley R, Hable WE, Kropf DL (2006) Polarization of the endomembrane system is an early event in fucoid zygote development. BMC Plant Boil **6**: 5

Harper S, Speicher DW (2011) Purification of proteins fused to glutathione S-transferase. Methods Mol Biol **681**: 259–280

Houbaert A, Zhang C, Tiwari M, Wang K, de Marcos Serrano A, Savatin DV, Urs MJ, Zhiponova MK, Gudesblat GE, Vanhoutte I, et al. (2018) POLAR-guided signalling complex assembly and localization drive asymmetric cell division. Nature **563**: 574–578

Humphries JA, Vejlupkova Z, Luo A, Meeley RB, Sylvester AW, Fowler JE, Smith LG (2011) ROP GTPases act with the receptor-like protein PAN1 to polarize asymmetric cell division in maize. Plant Cell **23**: 2273–2284

Kennard JL, Cleary AL (1997) Pre-mitotic nuclear migration in subsidiary mother cells of occurs in G1 of the cell cycle and requires F-actin. Cell Motil Cytoskelet **36**: 55–67

Kleine-Vehn J, Langowski L, Wisniewska J, Dhonukshe P, Brewer PB, Friml J (2008) Cellular and molecular requirements for polar PIN targeting and transcytosis in plants. Mol Plant **1**: 1056–1066

Kimata Y, Higaki T, Kawashima T, Kurihara D, Sato Y, Yamada T, Hasezawa S, Berger F, Higashiyama T, Ueda M (2016) Cytoskeleton dynamics control the first asymmetric cell division in Arabidopsis zygote. Proc Natl Acad Sci USA **113**: 14157–14162

Kodama Y, Suetsugu N, Wada M (2011) Novel protein-protein interaction family proteins involved in chloroplast movement response. Plant Signal Behav **6**: 483–490

Kodama Y, Suetsugu N, Kong SG, Wada M (2010) Two interacting coiled-coil proteins, WEB1 and PMI2, maintain the chloroplast photorelocation movement velocity in Arabidopsis. Proc Natl Acad Sci USA **107**: 19591–19596

Larkin MA, Blackshields G, Brown NP, Chenna R, McGettigan PA, McWilliam H, Valentin F, Wallace IM, Wilm A, Lopez R, et al. (2007) Clustal W and Clustal X version 2.0. Bioinformatics **23**: 2947–2948

Lee JS, Kuroha T, Hnilova M, Khatayevich D, Kanaoka MM, McAbee JM, Sarikaya M, Tamerler C, Torii KU (2012) Direct interaction of ligand–receptor pairs specifying stomatal patterning. Genes Dev **26**: 126–136

Lipka E, Herrmann A, Mueller S (2015) Mechanisms of plant cell division. Wiley interdisciplinary reviews. Dev Biol **4**: 391–405

Luesse DR, DeBlasio SL, Hangarter RP (2006) Plastid movement impaired 2, a new gene involved in normal blue-light-induced chloroplast movements in Arabidopsis. Plant Physiol **141**: 1328–1337

Mohanty A, Luo A, DeBlasio S, Ling X, Yang Y, Tuthill DE, Williams KE, Hill D, Zadrozny T, Chan A, et al. (2009) Advancing cell biology and functional genomics in maize using fluorescent protein-tagged lines. Plant Physiol **149**: 601–605

Muroyama A, Bergmann DC (2019) Plant cell polarity: creating diversity from inside the box. Annu Rev Cell Dev Biol **35**: 309–336

Muroyama A, Gong Y, Bergmann DC (2020) Opposing, polarity-driven nuclear migrations underpin asymmetric divisions to pattern Arabidopsis stomata. Curr Biol **30**: 4467–4475

Nakayama M, Kikuno R, Ohara O (2002) Protein-protein interactions between large proteins: two-hybrid screening using a functionally classified library composed of long cDNAs. Genome Res **12**: 1773–1784

Nan Q, Mendoza J, Facette M (2019) Double labeling of microtubules and actin filaments in maize leaf division zone. Bio-protocol **9**: e3262–e3262

Nunes TDG, Zhang D, Raissig MT (2020) Form, development and function of grass stomata. Plant J **101**: 780–799

Pillitteri LJ, Peterson KM, Horst RJ, Torii KU (2011) Molecular profiling of stomatal meristemoids reveals new component of asymmetric cell division and commonalities among stem cell populations in Arabidopsis. Plant Cell **23**: 3260–3275

Pillitteri LJ, Torii KU (2012) Mechanisms of stomatal development. Annu Rev Plant Biol **63**: 591–614

Romit Chakrabarty RB, Chung S-M, Farman M, Citovsky V, Hogenhout SA, Tzfira T, Goodin M (2006) pSITE vectors for stable integration or transient expression of autofluorescent protein fusions in plants: probing Nicotiana benthamiana–virus interactions Plant Physiol **20**: 740–750

Raissig MT, Matos JL, Anleu Gil MX, Kornfeld A, Bettadapur A, Abrash E, Allison HR, Badgley G, Vogel JP, Berry JA, et al. (2017) Mobile MUTE specifies subsidiary cells to build physiologically improved grass stomata. Science **355**: 1215–1218

Shao W, Dong J (2016) Polarity in plant asymmetric cell division: division orientation and cell fate differentiation. Dev Biol **419**: 121–131

Sowa ME, Bennett EJ, Gygi SP, Harper JW (2009) Defining the human deubiquitinating enzyme interaction landscape. Cell **138**: 389–403

Sugiyama Y, Nagashima Y, Wakazaki M, Sato M, Toyooka K, Fukuda H, Oda Y (2019) A Rho-actin signaling pathway shapes cell wall boundaries in Arabidopsis xylem vessels. Nat Commun **10**: 468

Stebbins GL, Shah SS (1960) Developmental studies of cell differentiation in the epidermis of monocotyledons. II. Cytological features of stomatal development in the Gramineae. Dev Biol **2**: 477–500

Tamura K, Peterson D, Peterson N, Stecher G, Nei M, Kumar S (2011) MEGA5: molecular evolutionary genetics analysis using maximum likelihood, evolutionary distance, and maximum parsimony methods. Mol Biol Evol **28**: 2731–2739

Wang K, Yang Z, Qing D, Ren F, Liu S, Zheng Q, Liu J, Zhang W, Dai C, Wu M, et al. (2018) Quantitative and functional posttranslational modification proteomics reveals that TREPH1 plays a role in plant touch-delayed bolting. Proc Natl Acad Sci USA **115**: E10265–E10274

Wu SZ, Bezanilla M (2018) Actin and microtubule cross talk mediates persistent polarized growth. J Cell Biol **217**: 3531–3544

Xiang Y, Huang X, Wang T, Zhang Y, Liu Q, Hussey PJ, Ren H (2007) ACTIN BINDING PROTEIN 29 from Lilium pollen plays an important role in dynamic actin remodeling. Plant Cell **19**: 1930–1946

Yang Z (2008) Cell polarity signaling in Arabidopsis. Annu Rev Cell Dev Biol **24**: 551–575

Yoshida S, van der Schuren A, van Dop M, van Galen L, Saiga S, Adibi M, Moller B, Ten Hove CA, Marhavy P, Smith R, et al. (2019) A SOSEKI-based coordinate system interprets global polarity cues in Arabidopsis. Nat Plants **5**: 160–166

Zhang D, Abrash EB, Nunes TD, Hidalgo I, Gil MXA, Jesenofsky B, Lindner H, Bergmann DC, Raissig MT (2022) Opposite polarity programs regulate asymmetric subsidiary cell divisions in grasses. bioRxiv. https://doi.org/10.1101/2022.04.24.489281

Zhang X, Facette M, Humphries JA, Shen Z, Park Y, Sutimantanapi D, Sylvester AW, Briggs SP, Smith LG (2012) Identification of PAN2 by quantitative proteomics as a leucine-rich repeat-receptor-like kinase acting upstream of PAN1 to polarize cell division in maize. Plant Cell **24**: 4577–4589

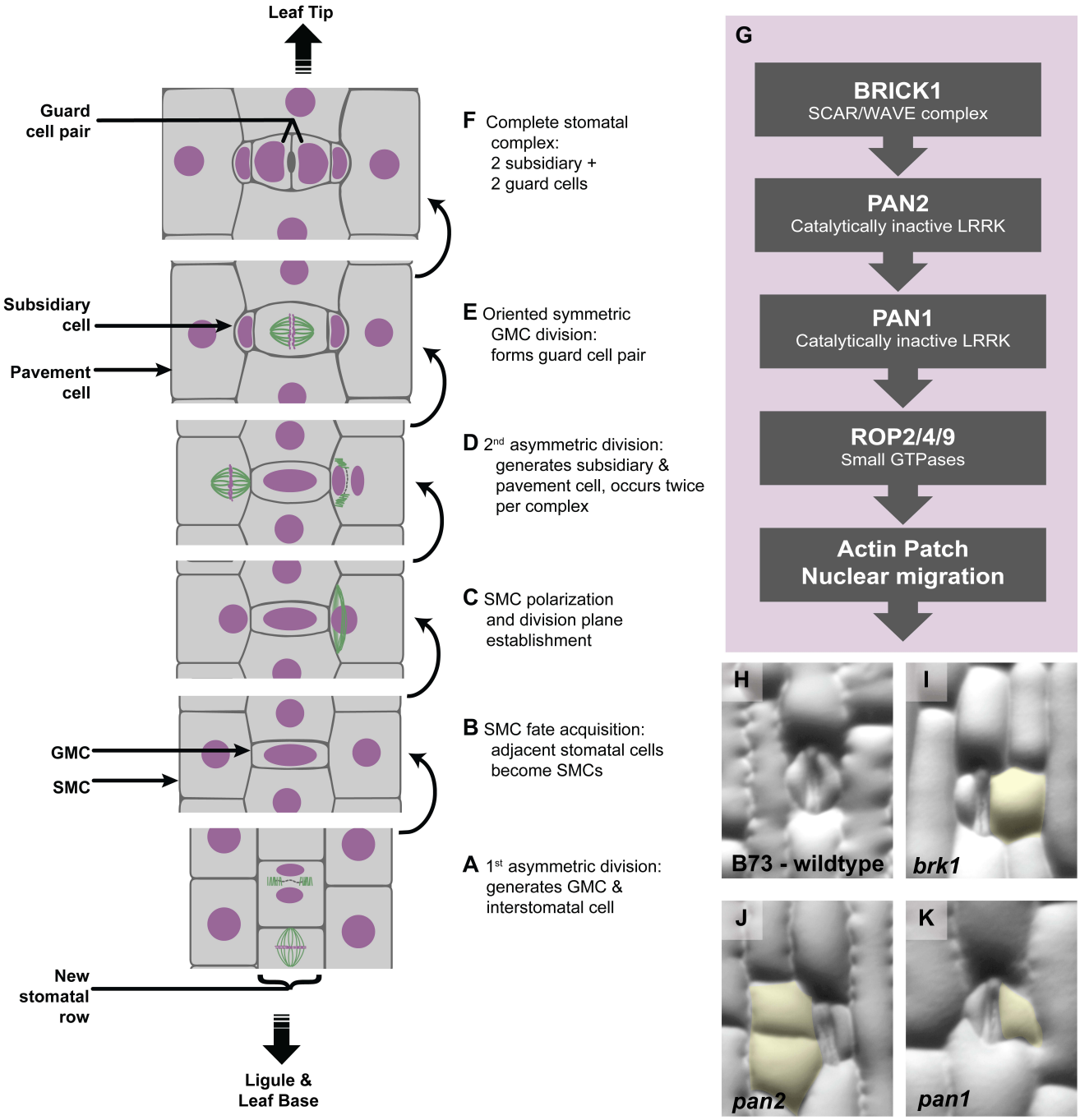

Supplemental Figure S1. Progression of maize stomatal development in leaves. Unexpanded maize leaves mature in a gradient with the developmentally youngest cells towards the base and the developmentally oldest cells towards the tip. **(A)** Stomatal complex formation is initiated by a transverse asymmetric division in a new stomatal row. **(B)** Pavement cells flanking the GMC acquire a SMC fate. At this stage, the nuclei are not yet polarized, but proteins (not shown) in the SMC may be polarized towards the GMC. **(C)** SMC nuclei polarize towards the GMC; preprophase band forms. **(D)** The SMCs divide, with each division forming **(E)** a subsidiary cell and a pavement cell. The GMC undergoes an oriented, symmetric division symmetrically to form (**F**), the guard cell pair. Each stomatal complex is made of two subsidiary and two guard cells. Nuclei/DNA are shown in magenta; microtubule structures are shown in green. **(G)** Ordered sequence of protein polarization, which occurs at the time shown in panel B. (**H-K**) Mutants with polarity defects result in abnormal subsidiary cells exhibit a range of abnormal morphologies. Examples of a single stomatal complex from wild type, *brk1, pan2,* and *pan1* mutants, where abnormal subsidiaries are false-colored yellow. Abbreviations: GMC: Guard Mother Cell. SMC: Subsidiary Mother Cell. LRRK: Leucine Rich Repeat Receptor Like Kinase. Supports Figures 1 and 5.

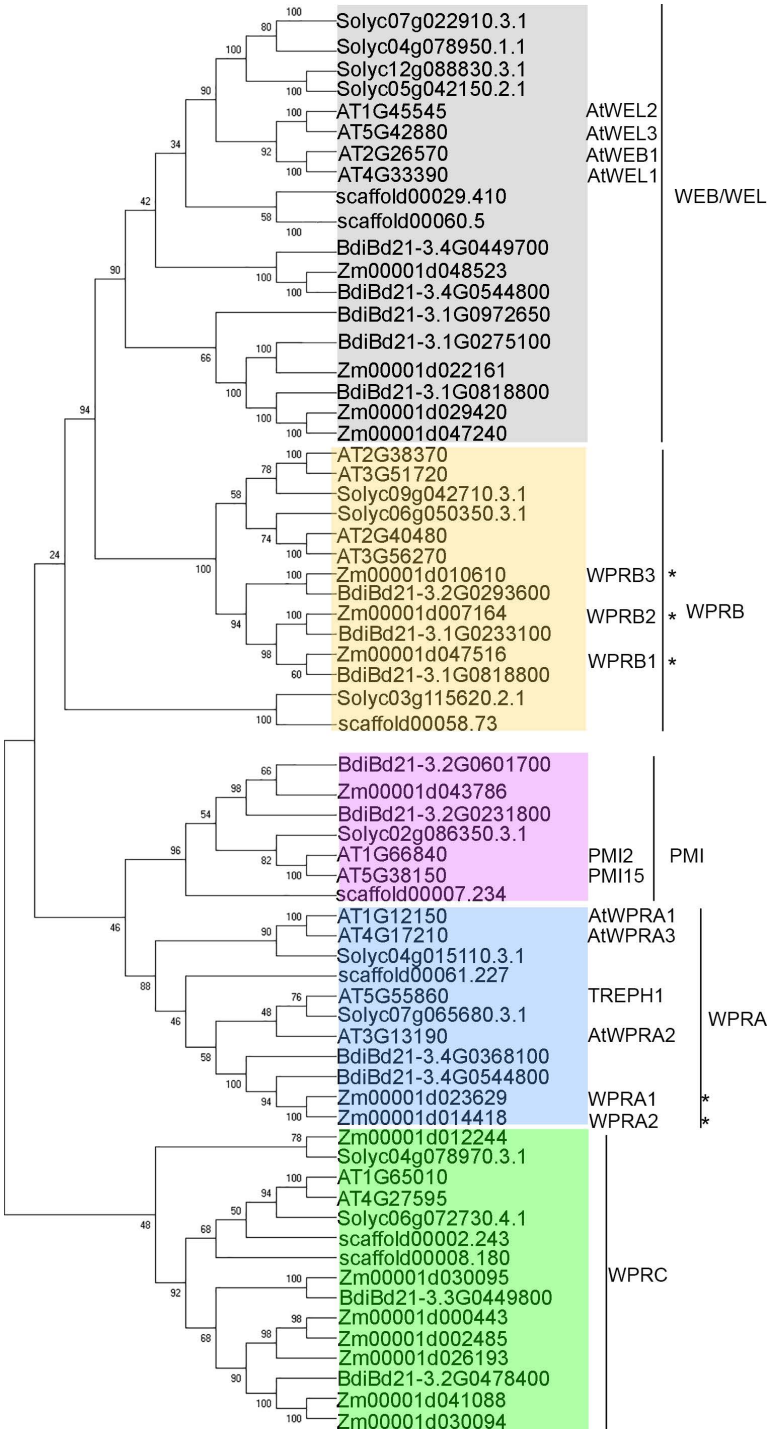

Supplemental Figure S2. Protein tree of the WPR family in plants. Protein coding sequences of WPR family members were identified from Phytozome 13 (https://phytozome-next.jgi.doe.gov/) from *A. thaliana* (dicot), *Amborella trichopoda* (dicot), *Solanum lycopersicum* (tomato, dicot), *B. distachyon* (monocot) and *Zea mays* (maize, monocot), and a protein tree was inferred. The proteins fall into 5 subfamilies, including the previously identified WEB/WEL, WPRB, WPRA and PMI clades – we also identified an additional WPRC clade. Previously named proteins are listed, and asterisks mark proteins characterized in this study. Protein sequences were aligned using Clustal Omega and the tree was inferred using MEGA 11. Numbers at nodes represent the percentage values given by 1000 bootstrap analysis samples. At: *Arabidopsis thaliana*, Zm: *Zea mays*. Bd: *Brachypodium distachyon,* Solyc: *Solanum lycopersicum*, scaffold: *Amborella trichopoda.* Supports Figure 1.

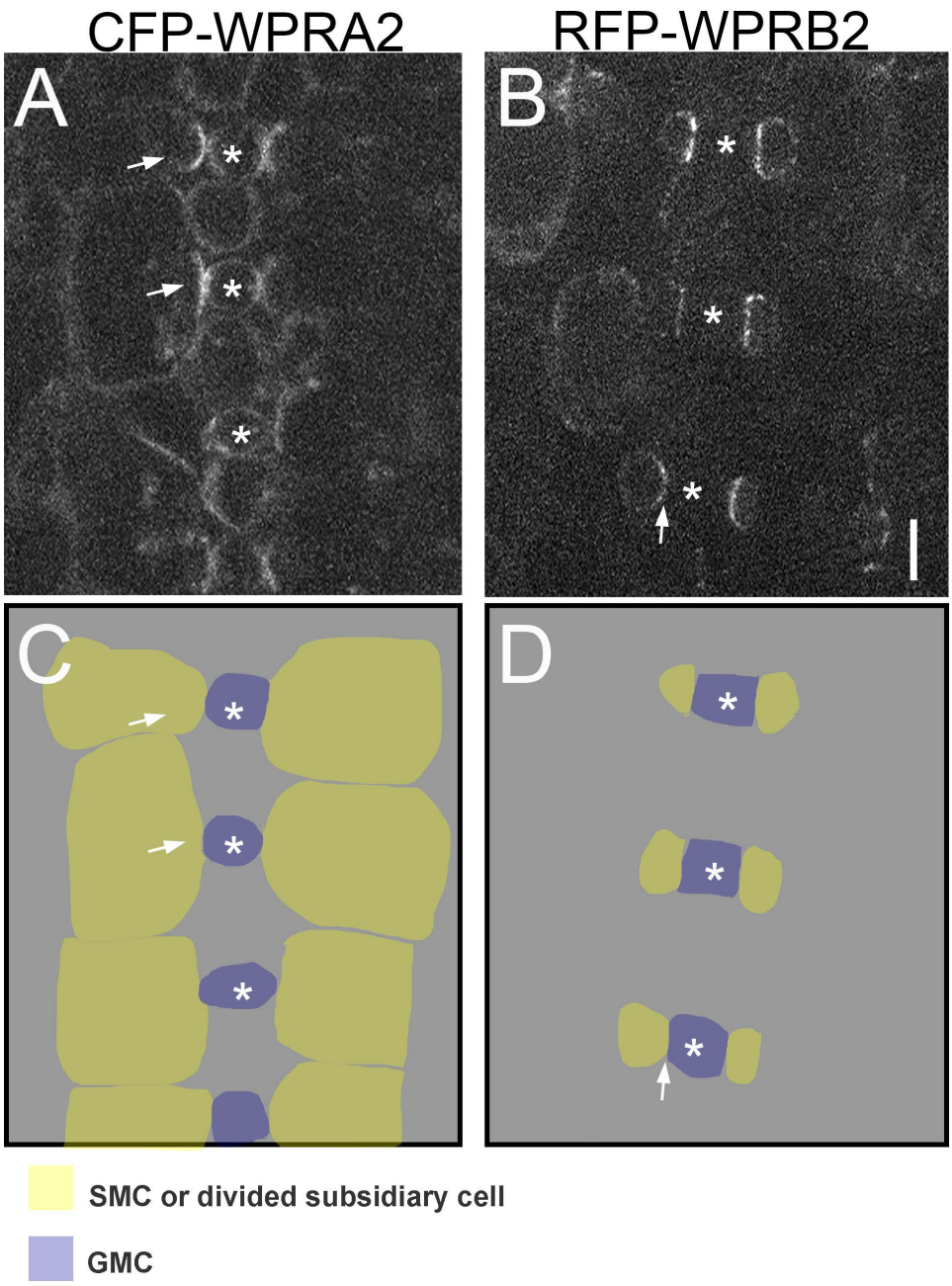

Supplemental Figure S3. **Plasmolysis assays of CFP-WPRA2 and RFP-WPRB2 transgenic plants.** Plants expressing either CFP-WPRA2 or RFP-WPRB2 were treated with 0.8M mannitol to induce plasmolysis, to determine if WPR proteins were primarily localized to SMCS or GMCs. Similar results were found with both fusions, with representative images shown. Although plasmolysis results in significant loss of overall signal, fluorescence was still visible in some cells, especially in SMCs. (A) CFP-WPRA2 expressing cells. Arrows point to bright fluorescent patches in two cells that are SMCS. Based on the curvature of the membrane, away from GMCs (marked by asterisks), the polarized fluorescence is predominantly in SMCs. Residual signal could also be seen in GMCs, although typically was much stronger in SMCs. (B) RFP-WRPB2 expressing cells. In these more mature cells, the SMCs have likely already divided, and polarized fluorescence remains in subsidiary cells. Arrow points to a cell where fluorescence is clearly seen in the subsidiary cell, but not the adjacent GMC. (C) and (D) are cartoon schematics of (A) and (B) respectively, with color-coding of cell types. GMC: Guard Mother Cell. SMC: Subsidiary Mother Cell. Scale bar = 10 μm. Supports Figure 1.

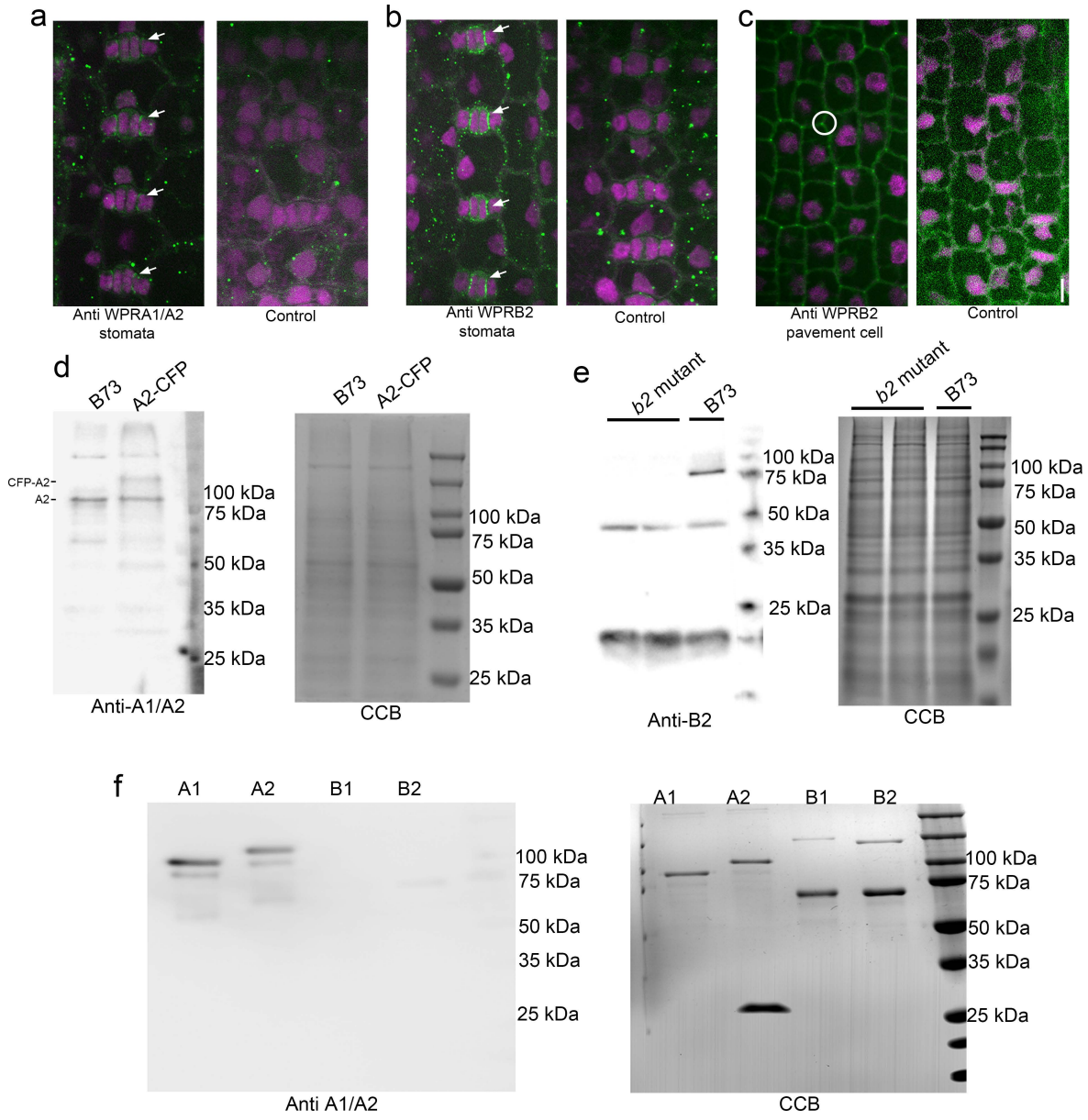

Supplemental Figure S4. **Immunolocalization using WPRA1/2 and WPRB2 antibodies and their validation (a)** Immunostaining with anti-WPRA1/A2 (green) antibodies and propidium iodide-staining (magenta) of developing leaf 4. No anti-WPRA1/A2 was used as a negative control. Arrows indicate the localization of WPRA1/A2 at the interface of subsidiary cells and guard cells. **(b and c)** Immunostaining with anti-WPRB2 (green) antibodies and propidium iodide (magenta). CRISPR-Cas9 induced *wprb2* mutants were used as a negative control. Arrows in (b) indicate the localization of WPRB2 at the interface of subsidiary cells and guard cells, in (c) indicate the localization of WPRB2 at pavement cell corner. **(d-f)** Confirmation of anti-WPRA1/A2 **(d and f)** and anti-WPRB2 **(e)** specificity using Western blotting. **(d)** Western blot of proteins extracted from B73 and CFP-WPRA2 transgenic plants probed with affinity-purified anti-WPRA1/A2. A band corresponding to the predicted size of endogenous WPRA1/A2 was recognized in B73. The same band was recognized in CFP-WPRA2 expressing plants; as was a larger band specific to the transgenic plants, which corresponds to the predicted size of CFP-WPRA2. In the right panel, Coomassie Brilliant Blue (CCB) staining of the gel is shown as a loading control. **(e)** Proteins extracted from *wprb2* mutants and B73 were used for western blotting assays. A band around 75 kD which consistent with the mass of WPRB2 protein was recognized in B73 but not in two *wprb2* mutants, Coomassie blue (CCB) staining is shown as a loading control. **(f)** Western blot of bacterially-expressed and purified GST-tagged WPRA1, WPRA2, WPRB1, WPRB2 proteins probed with affinity-purified WPRA1/A2 antibody demonstrates the specificity of this antibody for WPRA proteins. The Coomassie blue–stained gel (CCB) in the lower panel shows the purified proteins of WPRA1, WPRA2, WPRB1, WPRB2. Scale bar in c = 10 μm, all microscopy images scaled identically. Supports Figure 1, Figure 2 and Supplemental Dataset 2.

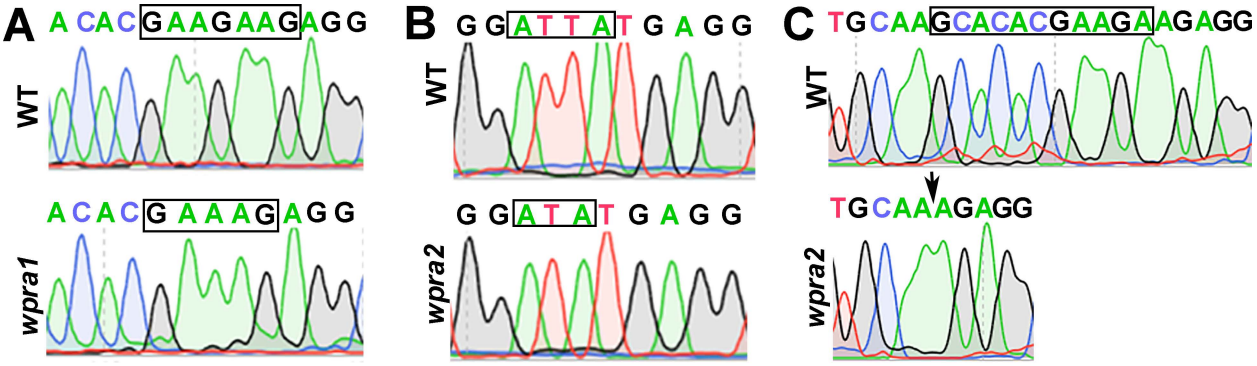

D

Parents	Progeny	Expected	Observated Ratio	χ^2 P Value
wpra1/+; wpra2/+ selfing	*a1_;a2_* : *a1_;a2/a2* : *a1/a1;a2_* : *a1/a1;a2/a2*	9:3:3:1	78:15:13:0	P < 0.01
wpra1/+; wpra2/wpra2 selfing	*+/+;a2/a2* : *a1/+;a2/a2* : *a1/a1;a2/a2*	1:2:1	38:48:0	P < 0.01

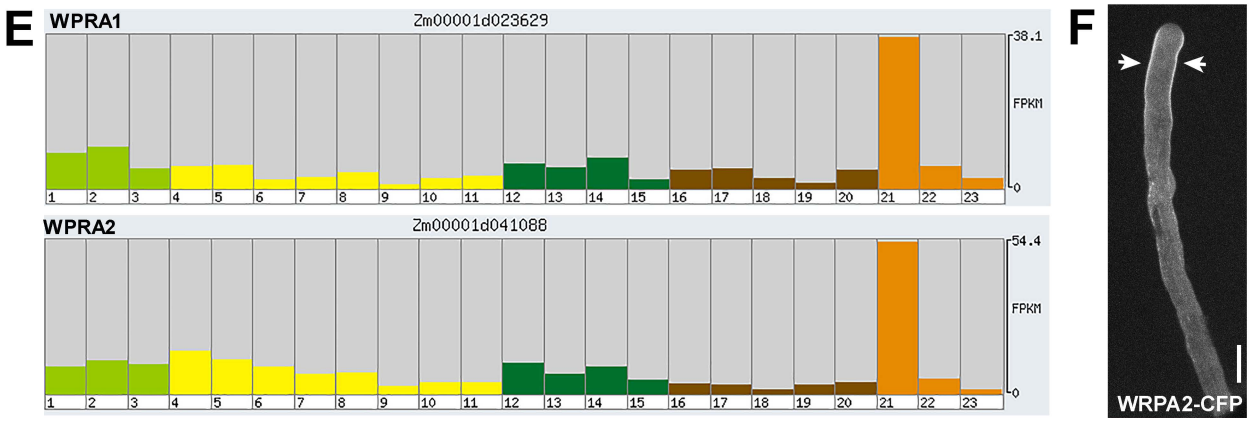

Supplemental Figure 5. CRISPR-Cas9 induced *wpra1 and wpra2* mutants have transmission defects. Mutated regions are labeled with black squares. **(A)** DNA sequences of Cas9-edited *Wpra1*. *wpra1* has a two nucleotide "GA" deletion at the gRNA2-targeted site. **(B)** and **(C)** DNA sequences of Cas9-edited *Wpra2,* Two mutations were identified: a "T" deletion was found at the gRNA1-targeted site (B), and an 11bp (GCACACGAAGA) deletion was found at gRNA2-targeted site (arrow, C). **(D)** Genotype analysis was performed in the progeny of *wpra1*/+; *wpra2*/+ and *wpra1*/+; *wpra2*/*wpra2* mutants. No *wpra1*/*wpra1*; *wpra2*/*wpra2* double mutants were recovered; observed ratios are significantly different from expected ratios. **(E)** RNA-seq expression level in maize growth stages (Data from MaizeGDB, Walley et al., 2016). Stage 21 is B73_Mature Pollen (expression level = 54.4). **(F)** CFP-WPRA2 localization in maize pollen tube. Maize pollen stably expressing CFP-WPRA2 were germinated in liquid culture for 1 hour at room temperature observed using spinning disk confocal and images were collected at × 60 objective (NA = 1.20, Olympus). The arrows point to subapex region localization of CFP-WPRA2. Scale bar in (F) = 10 μm. Supports Figure 5.

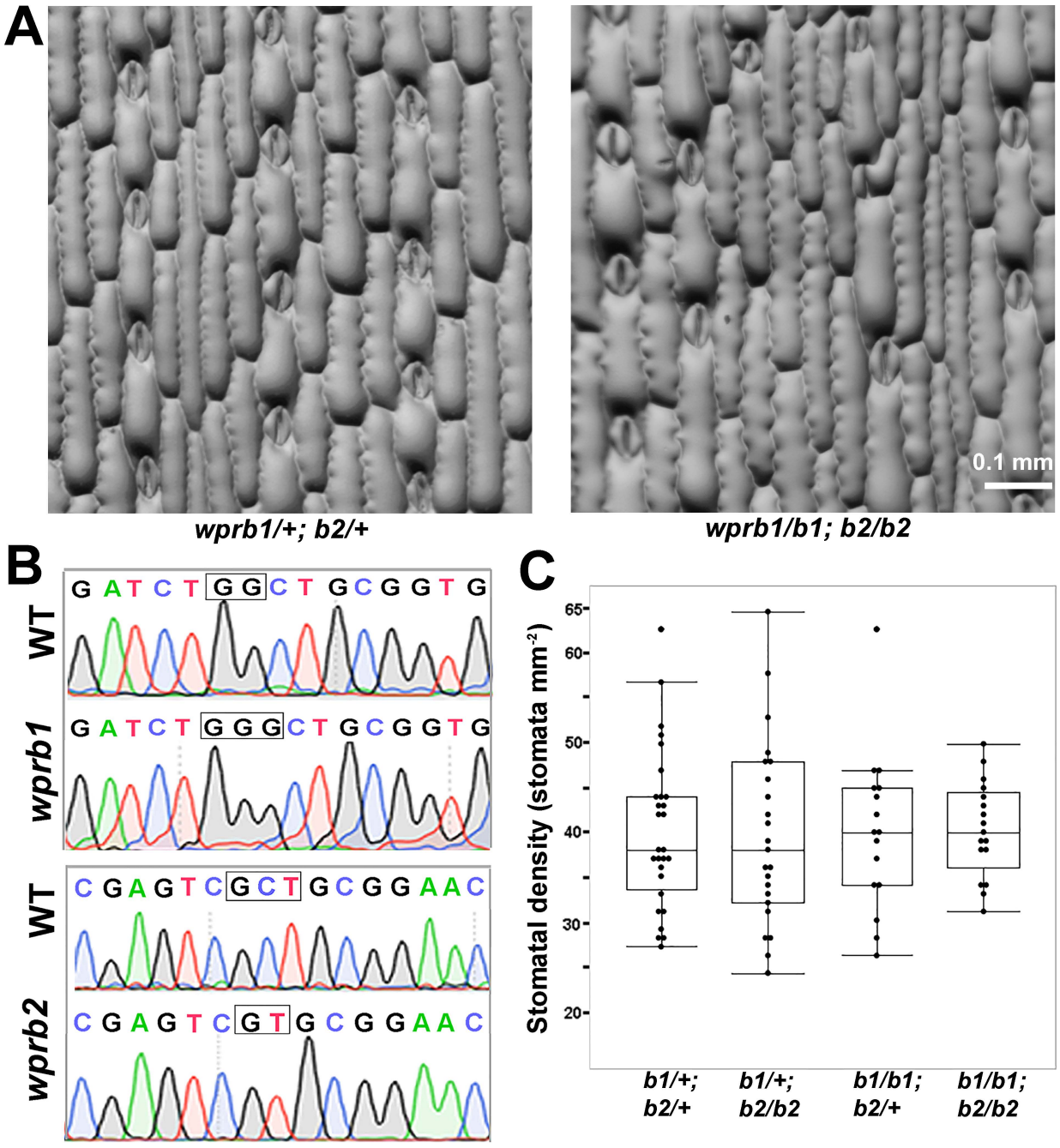

Supplemental Figure 6. CRISPR-Cas9 induced *wprb1;wprb2* double mutants have no effect on stomatal density. (A) Representative image of the third leaf of epidermis of *wprb1/+;wprb2/+* and *wprb1/b1;wprb2/b2* mutants. Scale bar, 0.1 mm. **(B)** Cas9-edited *Wprb1* and *Wprb2* genes. Mutated regions are labeled in black square; wprb1 has a "G" insertion and wprb2 has a "C" deletion in the gRNA targeted region. These mutations cause frameshifts and premature termination. **(C)** Quantification of stomatal density in *wprb1/+; wprb2/+* (n = 27 plants), *wprb1/b1;wprb2/+* (n = 14 plants), *wprb1/+;wprb2/wprb2* (n = 22 plants) and *wprb1/wprb1;wprb2/wprb2* (n=18 plants). Box plots show median values (center line), 25th to 75th interquartile range (box) and 1.5*interquartile range (whiskers). Student's T-tests were performed among these genotypes, no significant difference in these mutants. Supports Figure 5.

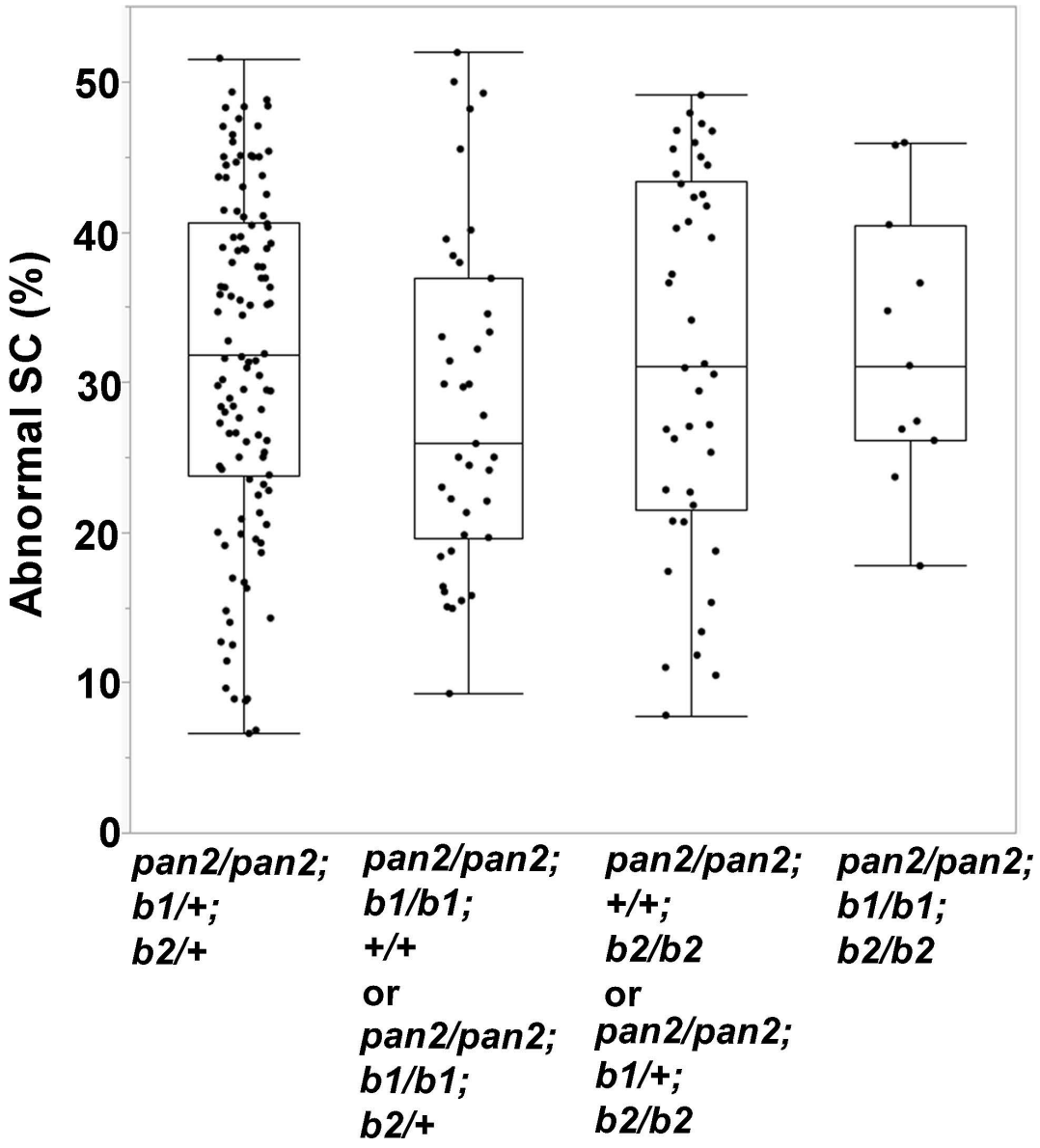

Supplemental Figure S7. Mutations in *wprb1* and *wprb2* do not enhance *pan2*/*pan2* phenotype. Stomatal phenotypes of progeny of *pan2*/*pan2; wprb1*/+*; wprb2*/+ plants were performed using the fully expanded third leaf. The percentage of abnormal subsidiary cell (SC) was quantified in different genotypes, *pan2/pan2; wprb1*/+*; wprb2/*+ (n = 113 plants)*, pan2/pan2; wprb1*/*wprb1;wprb2_*(n = 38 plants)*, pan2*/*pan2;wprb1_; wprb2*/*wprb2* (n= 41 plants) *and triple mutants pan2*/*pan2;wprb1*/*wprb1; wprb2*/*wprb2* (n= 11 plants). For each plant 100-200 subsidiary cells were genotyped. Box plots show median values (center line), 25th to 75th interquartile range (box) and 1.5*interquartile range (whiskers). ANOVA and pair-wise student's T-tests were performed among these genotypes with no significant differences. Supports Figure 5.

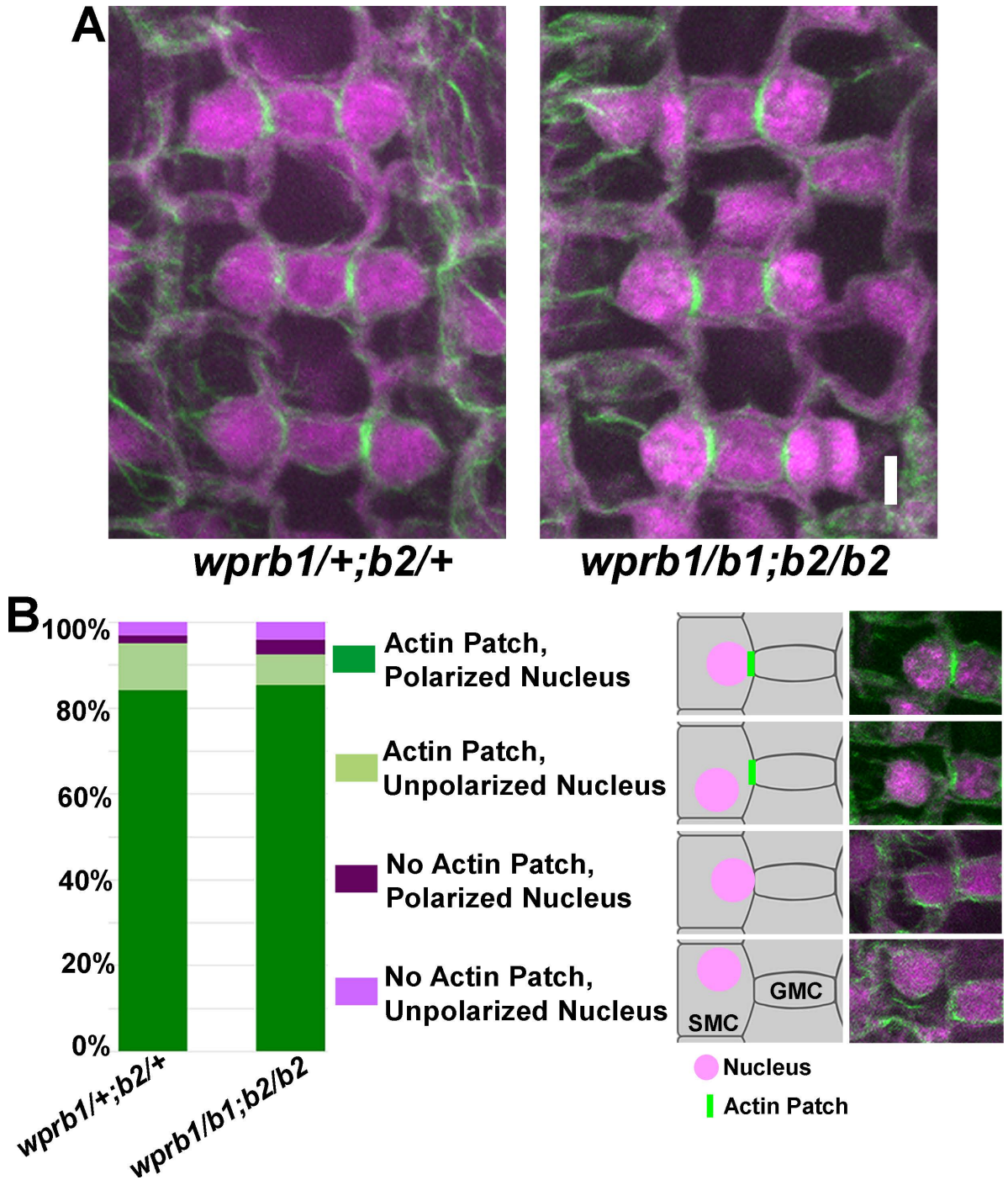

Supplemental Figure S8. CRISPR-Cas9 induced *wprb1;wprb2* double mutants have no effect on polarized actin accumulation or nuclear polarization during maize SMC development. The stomatal division zone of developing leaf 4 from *wprb1;wprb2* double mutants, and heterozygous siblings was stained using Alexafluor488-phalloidin (green) and propidium iodide (magenta). SMCs adjacent to GMCs that were greater than than 6 µm in width were used for the quantification, at this stage the majority of SMCs in wild-type had both actin patch and polarized nucleus at SMC-GMC interface. Cells were assayed for the presence of an actin patch, and whether the nucleus was polarized (touching the SMC-GMC interface). (A) Representative image of Alexafluor488-phalloidin stained actin (green) and propidium iodided stained DNA (magenta) in leaf epidermis from *wprb1/+;wprb2/+* and *wprb1/b1;wprb2/b2* plants. Bar = 5 µm. (B) Quantification of SMC classifications in *wprb1/+;wprb2/+* (n = 3 plants, 221 cells) and *wprb1/b1;wprb2/b2* (n = 3 plants, 241 cells) sibling plants. Supports Figure 5.

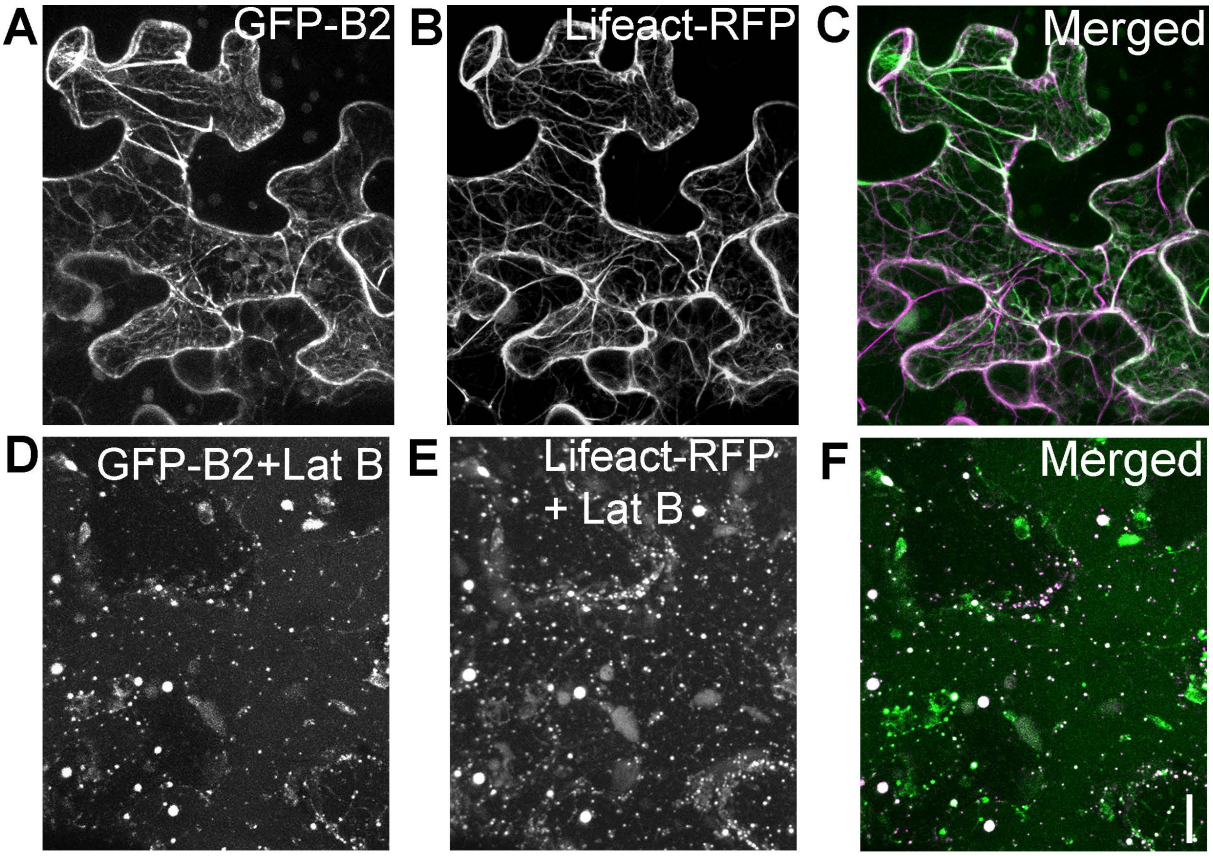

Supplemental Figure S9. Latrunculin B-treated tobacco leaf cells transiently expressing GFP-WPRB2 and Lifeact-RFP. Tobacco leaves co-expressing GFP-WPRB2 and Lifeact-RFP were treated with DMSO **(**negative control, **A-C)** or 40 µM Latrunculin B **(D-F)** for 2 hours. Scale bar in F = 20 µm. All images scaled identically. Supports Figure 6.

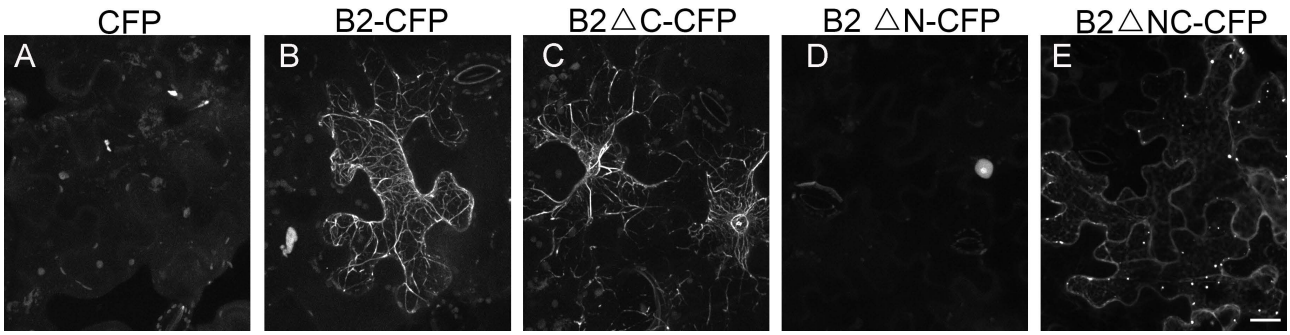

Supplement Figure S10. **Transient expression of WPRB2-CFP, and its truncated proteins.** Localization of WPRB2 in tobacco was confirmed using a CFP (rather than GFP) tag, and a C-terminal (rather than N-terminal) fusion. See Figure 6A for cartoon of protein truncations tested. (A) Soluble CFP. (B) Full length WPRB2-CFP. (C) C-terminal truncation WPRB2ΔC-CFP (D) N-terminal truncation WPRB2ΔN-CFP localizes predominantly to the nucleus. (E) Central DUF827 domain only WPRB2ΔNC. Filaments structures appears in WPRB2-CFP and WPRB2△C-CFP expressing tobacco cells, but not in WPRB2ΔN-CFP and WPRB2ΔNC-CFP expressing tobacco cells. Scale bar in E = 20 μm. All images scaled identically. Supports Figure 6.

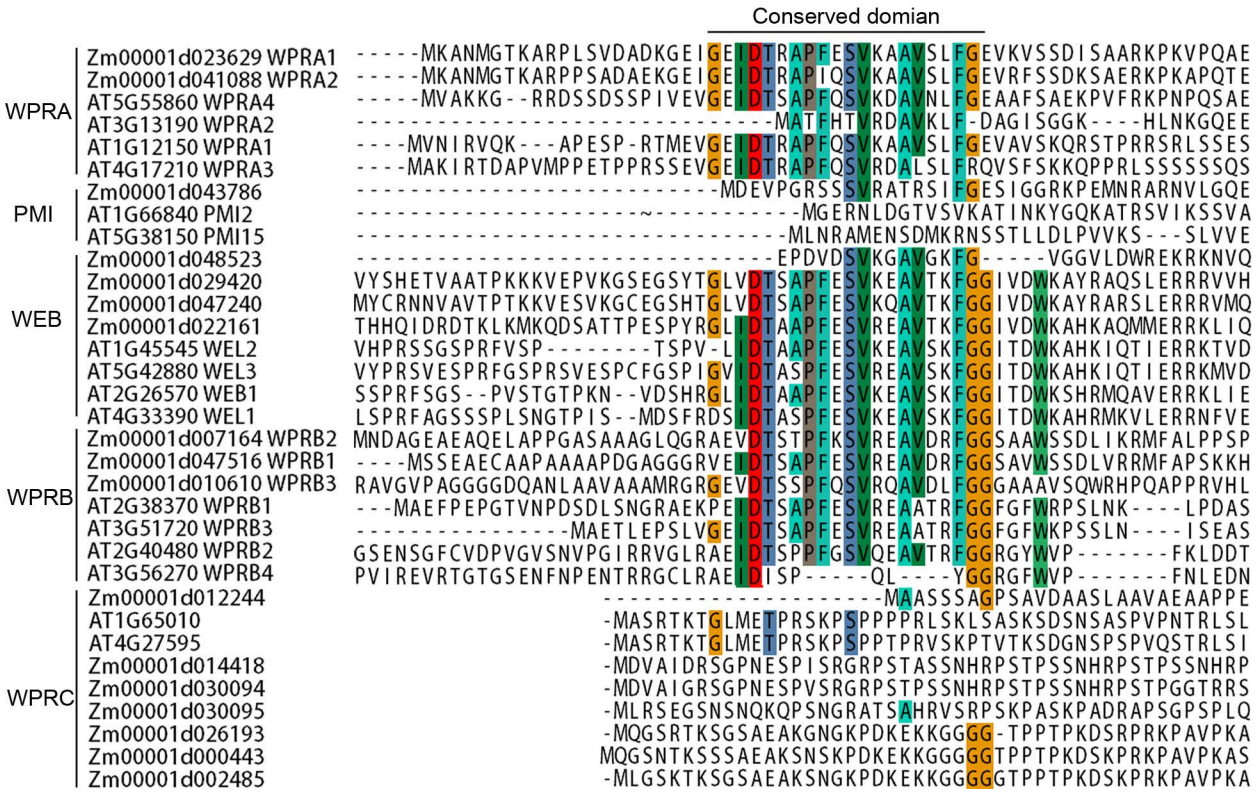

Supplemental Figure S11. Alignment of the actin-binding domain of the WPR protein family. The N terminal amino acids sequence WPRs from Arabidopsis and maize were aligned using ClustalX 2.0.5 (Larkin et al., 2007) with the default settings. Supports Figure S6.

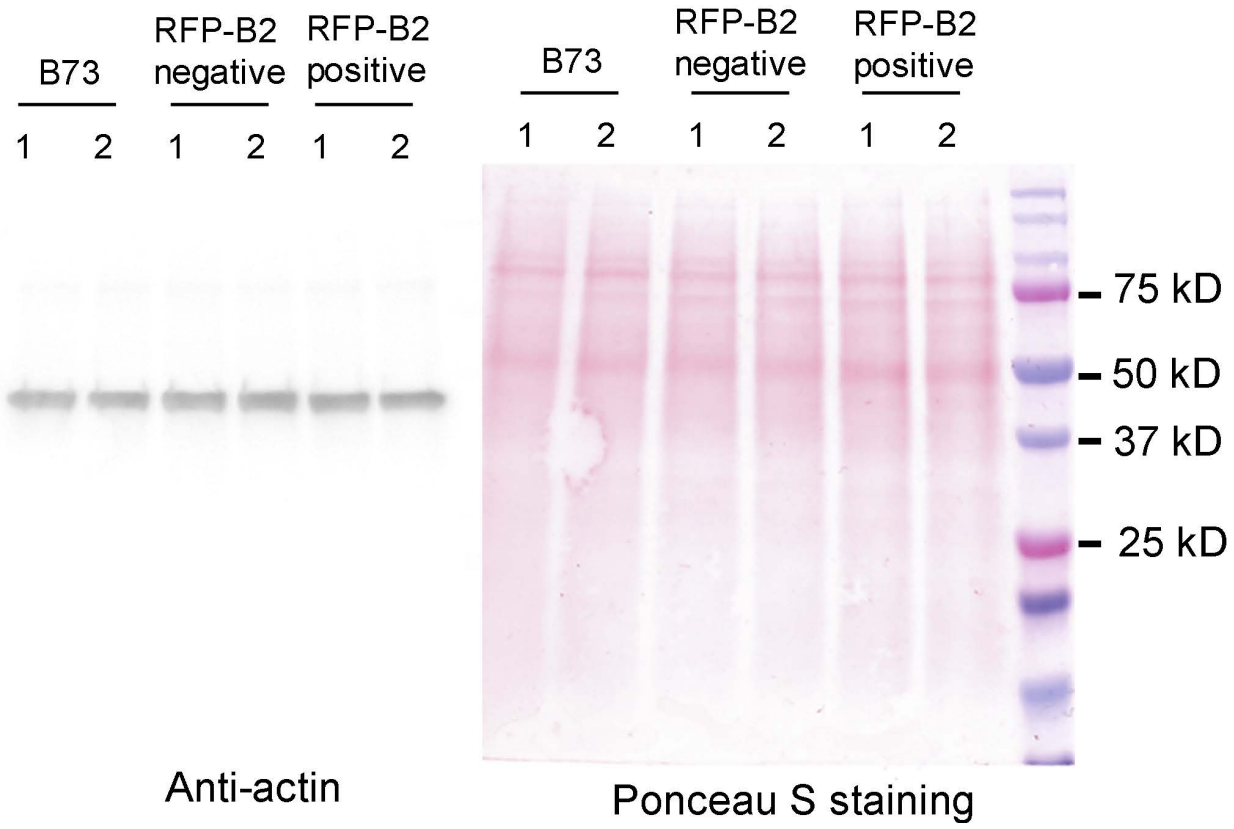

Supplemental Figure S12. RFP-WPRB2 expression has no effect on the total amount of actin. Western blot of total proteins extracted from the stomatal division zone of two independent plants of B73, RFP-WPRB2 transgenic plants, RFP negative siblings. Extracts were probed with an anti-actin antibody. Ponceau S staining is shown as a loading control.

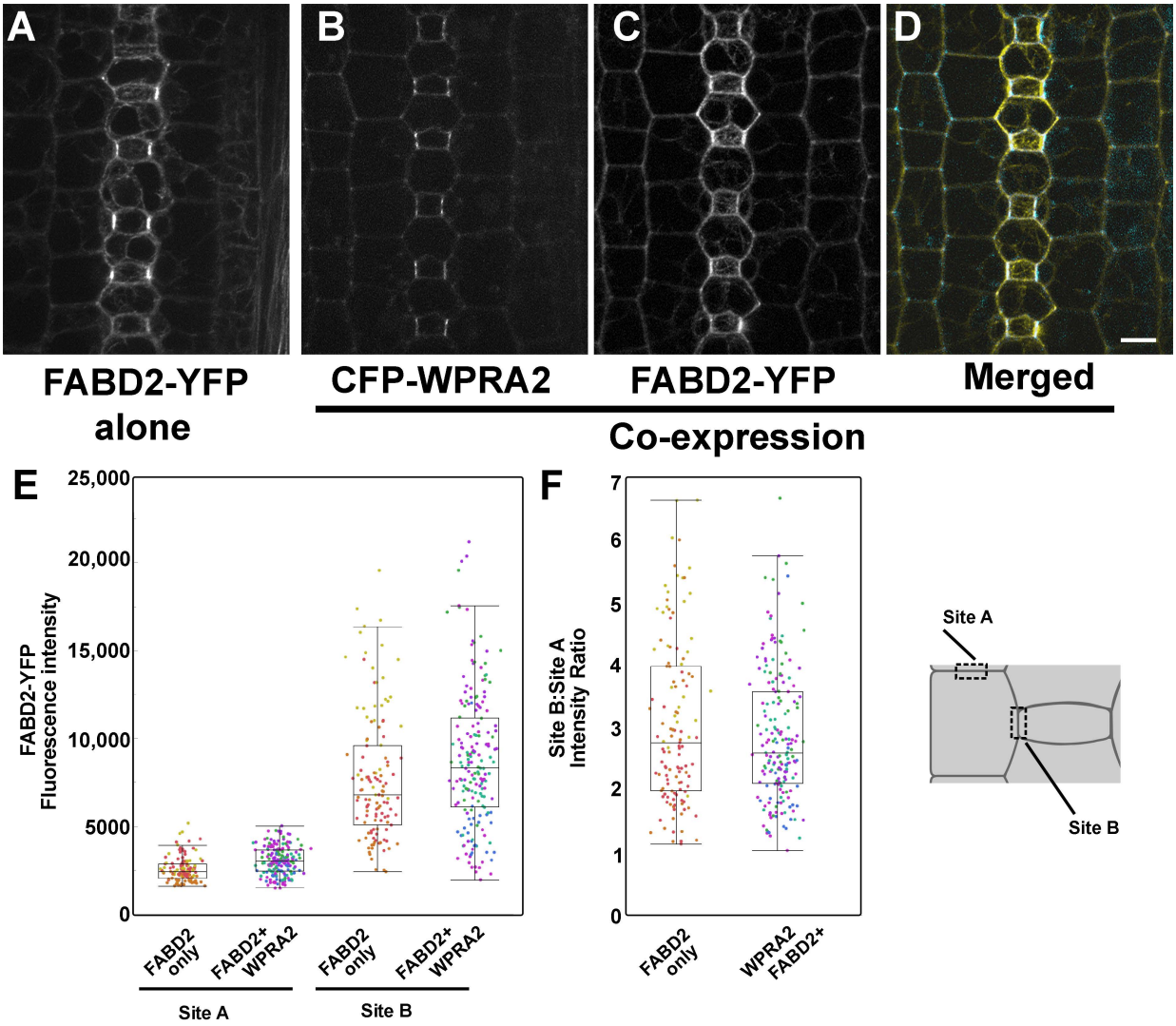

Supplemental Figure S13. Co-expression of CFP-WPRA2 with ABD2-YFP does not decrease FABD2-YFP intensity. Plants expressing CFP-WPRA2 and FABD2-YFP were crossed, and the progeny independently segregated the two markers. **(A)** Representative image of plant only expressing FABD2-YFP. **(B-D)** Plant co-expressing FABD2-YFP (yellow in D) **(C)** with CFP-WPRA2 (cyan in E) and the merged image **(D),** Scale bar in (D) = 10 µm, all images scaled identically. Images are 7-slice max projections. **(E, F)** Quantification of fluorescence intensity and intensity ratio of SMC lateral cell side (site A) and SMC-GMC interface (site B) in FABD2-YFP only plants (n = 3 plants, 254 cells) and CFP-WPRA2 + FABD2-YFP co-expressing plants (n = 5 plants, 379 cells). Dots of the same color are from the same plant. In E and F, box plots show median values (center line), 25th to 75th interquartile range (box) and 1.5*interquartile range (whiskers). Supports Figure 7.

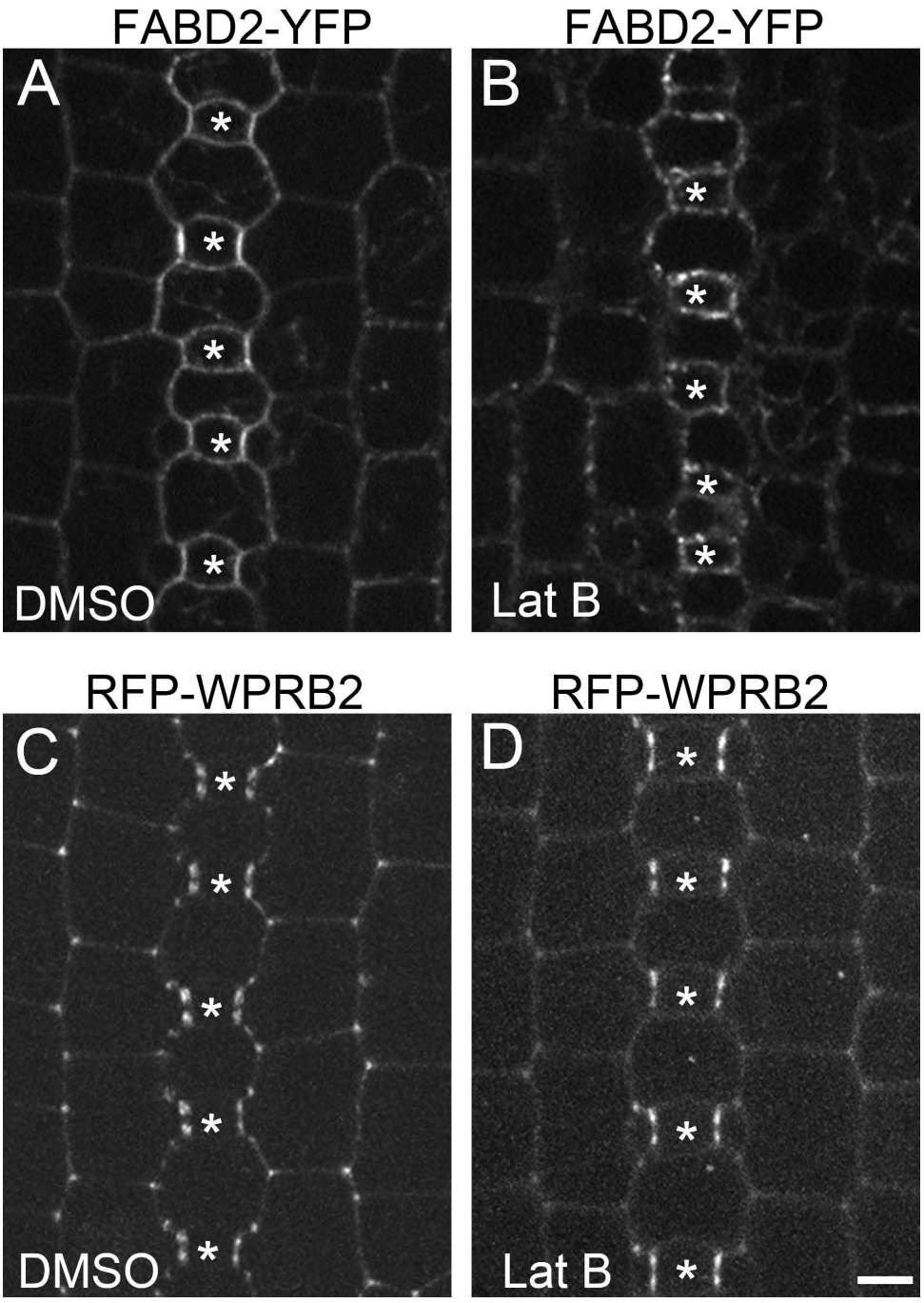

Supplemental Figure S14. **F-actin disruption does not affect the polarized localization of RFP-WPRB2 in SMCs**.**(A)** FABD2-YFP expressing maize leaves were treated with DMSO (negative control) and 40 μM Latrunculin B (Lat B) for 4 hours. **(B)** RFP-WPRB2 expressed maize leaves were treated with DMSO (negative control) and 40 μM Latrunculin B for 4 hours. Asterisks mark guard mother cells. Scale bar in D = 10 μm. All images scaled identically.

Supplemental Table 1. Primer sequences used in this study.

Primer name	Sequence (5'-3')	Description
WPRA2-F	GGGGACA AGTTTGTACAAAAAAGCAGGCTGC ATAACCATTTTATGCTTCAAGC	Primers for *Wpra2* promoter and 5' UTR amplification
WPRA2-R	GGGG AC CAC TTT GTA CAA GAA AGC TGG GTA GAAGTTGCAATTACACCTCTTTGT	
WPRA2-P2	GCTCCACCTCCACCTCCCATTTATTTAAATA TTTTACGC	Primers for *Wpra2* coding region and 3' UTR amplification
WPRA2-P3	GCTGCTGCGGCCGCTGGGGCCATGAAGGC AAATATGGGCAC	
WPRB2-F	GGGGACAAGTTTGAAAAAAGCAGGCTGCGA GATTCGAGACAACATACATG	Primers for *Wprb2* promoter and 5' UTR amplification
WPRB2-R	GGGGACCACTTTGTACAAGAAAGCTGGGTA TAAAACTCTCACACGAGAGATAC	
WPRB2-P2	GCTCCACCTCCACCTCCCATGGGGACTCGT GCCCCTCT	Primers for *Wprb2* coding region and 3' UTR amplification
WPRB2-P3	GCTGCTGCGGCCGCTGGGGCCATGAACGA CGCCGGCGAGGCCG	
Tag linker-F	ATGGGAGGTGGAGGTGGAGCT	Primers for CFP or RFP amplification
Tag linker-R	GGCCCCAGCGGCCGCAGCAGC	
WPRB2 topo-F	CACCATGAACGACGCCGGCGAGG	Primers for WPRB2N67 amplification
WPRB2N topo (1-67)-R	CTTTGGGCTCGGGGGCAGCG	
WPRB2N topo (1-142)-R	AGCGGCAGTGGGCAGCTCGGCTTG	WPRB2N142 R primer
WPRB2F-GW	GGGGACAAGTTTGTACAAAAAAGCAGGCTG CGC ATGAACGACGCCGGCGAGG	Primers for WPRB2 without stop code amplification
WPRB2R-GW(no stop code)	GGGGACCACTTTGTACAAGAAAGCTGGGTA ATGCGATCCCTTTTCCTTCTTC	
WPRB2 △N F-GW	GGGGACAAGTTTGTACAAAAAAGCAGGCTG C GCCGCTGAAGAGGTTGCAGAAG	Primers for WPRB2△C, WPRB2△N,WPRB2△NC amplification
WPRB2 △C R-GW	GGGGACCACTTTGTACAAGAAAGCTGGGTA CCTGTGTCCAGTCGTGGATCG	
WPRA1 topo-F	CACCATGAAGGCAAATATGGGC	Primers for WPRA1 CDS

WPRA1 topo-R	TCACACAGATTTTTCCCCAGGAAG	amplification
WPRA2 topo-F	CACCATGGGGTGGGGAAGAGCA	Primers for WPRA2 CDS amplification
WPRA2 topo-R	TTACACAGATTTTTCCCCAGGAAG	
WPRB1 topo-F	CACCATGAGCTCCGAAGCAGAA	Primers for WPRB1 CDS amplification
WPRB1 topo-R	TTAAAAGGATTCTCTCTTCTT	
WPRB2 topo-F	CACCATGAACGACGCCGGCGAG	Primers for WPRB2 CDS amplification
WPRB2 topo-R	CTAATGCGATCCCTTTTC	
WPRB3 topo-F	CACC ATGGCGGAAGTGGCGGCGCGGC	Primers for WPRB3 CDS amplification
WPRB3 topo-R	GCTCAAGCCACCACGAGTGCAGGAG	
WPRA1 BamHI 63F	CGCGGATCC TTAGCCAAGGAGACAGA	Primers of WPRA1(63-503) amplification and GST-WPRA1 expression
WPRA1 EcorI 503R	CCGGAATTC CAACTTCTCTGACTC	
WPRA2 BamHI 63F	CGCGGATCC TTAGCCAAGGAGACAGA	Primers of WPRA1(63-570) amplification and GST-WPRA2 expression
WPRA2 EcorI 570R	CCGGAATTC CTTCTCGCGCCATCT	
WPRB1 BamHI 73F	CGCGGATCC GCCGAGGAGCAGGCT	Primers of WPRB1(73-421) amplification and GST-WPRB1 expression
WPRB1 EcorI 421R	CCGGAATTC TTACCCGCTCTCAGATTT	
WPRB2 BamHI 78F	CGCGGATCC GAGGAGCAGACCGCG	Primers of WPRA1(78-429) amplification and GST-WPRB2 expression
WPRB2 EcorI 429R	CCGGAATTC GGATCGACATCTGCG	
WPRB2 BamHI F	CGCGGATCCATGAACGACGCCGGCGAG	Primers of WPRB2N240 amplification and GST-WPRB2N240 expression
WPRB2 N240 EcorI R	CCGGAATTCTTACTTCTGTGCAGTCCGGTTCAGCTC	

Suppplemental Table 2. Relates to **Figure 5G.** CRISPR-Cas9 induced *wprb1*;*wprb2* double mutants and CFP-WPRA2 and RFP-WPRB2 overexpression lines have subsidiary cell defects. ANOVA P<0.0001. Pair-wise t-tests (alpha =0.05) indicates the homozygous double mutant is different from all other genotypes; other genotypes do not differ from each other.

Analysis of Variance

Source	DF	Sum of Squares	Mean Square	F Ratio	Prob > F
genotype	3	310.51949	103.506	42.7373	<.0001*
Error	77	186.48795	2.422		
C. Total	80	497.00743			

Means for Oneway Anova

Level	Number	Mean	Std Error	Lower 95%	Upper 95%
b1/+; b2/b2	22	1.72122	0.33179	1.0605	2.3819
b1/+;b2/+	27	2.09320	0.29950	1.4968	2.6896
b1/b1; b2/+	14	2.46597	0.41593	1.6378	3.2942
b1/b1; b2/b2	18	6.71878	0.36681	5.9884	7.4492

Std Error uses a pooled estimate of error variance

Connecting Letters Report

Level		Mean
b1/b1; b2/b2	A	6.7187759
b1/b1; b2/+	B	2.4659659
b1/+;b2/+	B	2.0932006
b1/+; b2/b2	B	1.7212188

Levels not connected by same letter are significantly different.

Supplemental Table 3. Relates to **Figure 5H**. CRISPR-Cas9 induced *wprb1*;*wprb2* double mutants and CFP-WPRA2 and RFP-WPRB2 overexpression lines have subsidiary cell defects.

Means and Std Deviations

Level	Number	Mean	Std Dev	Std Err Mean	Lower 95%	Upper 95%
CFP-A2	12	2.8529194	1.0535671	0.3041386	2.1835148	3.522324
non-transgenic sibling	12	1.2614693	0.8428852	0.24332	0.7259256	1.797013

t Test

non-transgenic sibling-CFP-A2
Assuming unequal variances

Difference	-1.5915	t Ratio	-4.08595
Std Err Dif	0.3895	DF	20.98896
Upper CL Dif	-0.7814	Prob > |t|	0.0005*
Lower CL Dif	-2.4015	Prob > t	0.9997
Confidence	0.95	Prob < t	0.0003*

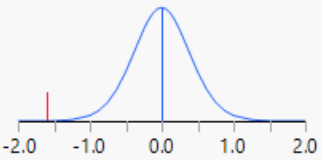

Supplemental Table 4. Relates to **Figure 5I**. CRISPR-Cas9 induced *wprb1*;*wprb2* double mutants and CFP-WPRA2 and RFP-WPRB2 overexpression lines have subsidiary cell defects.

Means and Std Deviations

Level	Number	Mean	Std Dev	Std Err Mean	Lower 95%	Upper 95%
B2RFP	12	4.5517755	1.7773618	0.5130801	3.4224937	5.6810573
noFP sibling	11	2.2333674	1.1677496	0.3520897	1.4488626	3.0178722

t Test

noFP sibling-B2RFP
Assuming unequal variances

Difference	-2.3184	t Ratio	-3.72573
Std Err Dif	0.6223	DF	19.13233
Upper CL Dif	-1.0166	Prob > |t|	0.0014*
Lower CL Dif	-3.6202	Prob > t	0.9993
Confidence	0.95	Prob < t	0.0007*

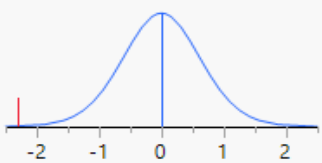

Supplemental Table 5. Chi–squared test relating to Supplemental Figure 5D, top row.

P value and statistical significance:

Chi squared equals 15.862 with 3 degrees of freedom.

The two-tailed P value equals 0.0012

By conventional criteria, this difference is considered to be very statistically significant.

The P value answers this question: If the theory that generated the expected values were correct, what is the probability of observing such a large discrepancy (or larger) between observed and expected values? A small P value is evidence that the data are not sampled from the distribution you expected.

Review your data:

Row #	Category	Observed	Expected #	Expected
1	a1_:a2_	78	59.625	56.250%
2	a1_:a2/a2	15	19.875	18.750%
3	a1/a1:a2_	13	19.875	18.750%
4	a1/a1;a2/a2	0	6.625	6.250%

Supplemental Table 6. Chi–squared test relating to Supplemental Figure 5D, bottom row.

P value and statistical significance:

Chi squared equals 34.744 with 2 degrees of freedom.

The two-tailed P value is less than 0.0001

By conventional criteria, this difference is considered to be extremely statistically significant.

The P value answers this question: If the theory that generated the expected values were correct, what is the probability of observing such a large discrepancy (or larger) between observed and expected values? A small P value is evidence that the data are not sampled from the distribution you expected.

Review your data:

Row #	Category	Observed	Expected #	Expected
1	+/+:a2/a2	38	21.5	25.000%
2	a1/+:a2/a2	48	43	50.000%
3	a1/a1;a2/a2	0	21.5	25.000%

Supplemental Table 7. Relates to **Supplemental Figure 7.** Mutations in *wprb1* and *wprb2* do not enhance *pan2*/*pan2* phenotype.ANOVA P=0.4758. Pair-wise t-tests (alpha =0.05) indicates the homozygous triple mutant is not different from siblings

Analysis of Variance

Source	DF	Sum of Squares	Mean Square	F Ratio	Prob > F
genotype	3	328.029	109.343	0.8355	0.4758
Error	202	26435.474	130.869		
C. Total	205	26763.503			

Means for Oneway Anova

Level	Number	Mean	Std Error	Lower 95%	Upper 95%
b1/+;b2/+	114	31.6553	1.0714	29.543	33.768
b1/+;b2/b2 or +/+; b2/b2	42	31.6667	1.7652	28.186	35.147
b1/b1; b2/b2	11	32.4062	3.4492	25.605	39.207
b1/b1;b2/+ or b1/b1; +/+	39	28.5149	1.8318	24.903	32.127

Std Error uses a pooled estimate of error variance

Connecting Letters Report

Level		Mean
b1/b1; b2/b2	A	32.406159
b1/+;b2/b2 or +/+; b2/b2	A	31.666667
b1/+;b2/+	A	31.655347
b1/b1;b2/+ or b1/b1; +/+	A	28.514937

Levels not connected by same letter are significantly different.

Supplemental Table 8. Relates **to Supplemental Figure 6.** CRISPR-Cas9 induced *wprb1;wprb2* double mutants have no effect on stomatal density.

Analysis of Variance

Source	DF	Sum of Squares	Mean Square	F Ratio	Prob > F
Genotype	3	3.3181	1.1060	0.0148	0.9975
Error	80	5987.4823	74.8435		
C. Total	83	5990.8004			

Means for Oneway Anova

Level	Number	Mean	Std Error	Lower 95%	Upper 95%
b1/+;b2/+	28	40.1786	1.6349	36.925	43.432
b1/+;b2/b2	23	39.7843	1.8039	36.194	43.374
b1/b1;b2/+	16	40.1001	2.1628	35.796	44.404
b1/b1;b2/b2	17	40.3263	2.0982	36.151	44.502

Std Error uses a pooled estimate of error variance

Supplemental Table 9 Relates to **Figure 7F.** Fluorescence intensity of ABD2-YFP decreases in RFP-WPRB2 expressing plants **(Site A)**

Means and Std Deviations

Level	Number	Mean	Std Dev	Std Err Mean	Lower 95%	Upper 95%
ABD2-YFP only	146	2256.6939	1124.8469	93.092988	2072.6994	2440.6885
B2-RFP + ABD2-YFP	82	1019.4439	127.24151	14.051474	991.48583	1047.4019

t Test

B2-RFP + ABD2-YFP-ABD2-YFP only
Assuming unequal variances

Difference	-1237.3	t Ratio	-13.1416
Std Err Dif	94.1	DF	151.5415
Upper CL Dif	-1051.2	Prob > |t|	<.0001*
Lower CL Dif	-1423.3	Prob > t	1.0000
Confidence	0.95	Prob < t	<.0001*

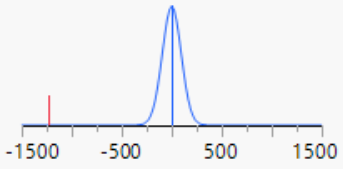

Supplemental Table 10. Relates to **Figure 7F.** Fluorescence intensity of ABD2-YFP decreases in RFP-WPRB2 expressing plants **(Site B)**

Means and Std Deviations

Level	Number	Mean	Std Dev	Std Err Mean	Lower 95%	Upper 95%
ABD2-YFP only	146	6867.4486	4709.4575	389.75748	6097.1087	7637.7884
B2-RFP + ABD2-YFP	82	1354.9146	334.39911	36.928204	1281.439	1428.3901

t Test

B2-RFP + ABD2-YFP-ABD2-YFP only
Assuming unequal variances

Difference	-5512.5	t Ratio	-14.0804
Std Err Dif	391.5	DF	147.5937
Upper CL Dif	-4738.9	Prob > |t|	<.0001*
Lower CL Dif	-6286.2	Prob > t	1.0000
Confidence	0.95	Prob < t	<.0001*

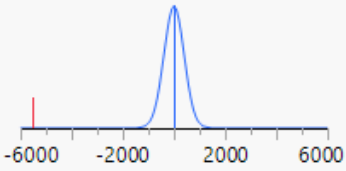

Supplemental Table 11.Relates to **Figure 7G.** Fluorescence intensity of ABD2-YFP decreases in RFP-WPRB2 expressing plants

Means and Std Deviations

Level	Number	Mean	Std Dev	Std Err Mean	Lower 95%	Upper 95%
ABD2-YFP only	146	2.9468289	1.1262941	0.0932128	2.7625977	3.1310602
B2-RFP + ABD2-YFP	82	1.3296136	0.2738226	0.0302386	1.2694482	1.3897791

t Test

B2-RFP + ABD2-YFP-ABD2-YFP only
Assuming unequal variances

Difference	-1.6172	t Ratio	-16.5031
Std Err Dif	0.0980	DF	173.6816
Upper CL Dif	-1.4238	Prob > |t|	<.0001*
Lower CL Dif	-1.8106	Prob > t	1.0000
Confidence	0.95	Prob < t	<.0001*

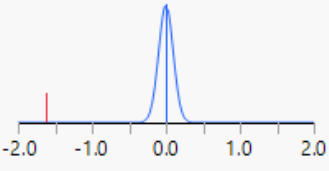

Supplemental Table 12. Relates to **Supplemental Figure 13A.** Co-expression of CFP-WPRA2 with ABD2-YFP does not decrease FABD2-YFP intensity **(Site A)**

Means and Std Deviations

Level	Number	Mean	Std Dev	Std Err Mean	Lower 95%	Upper 95%
ABD2-YFP	127	2565.2806	691.81757	61.388882	2443.7938	2686.7674
ABD2-YFP + CFP-A2	189	3046.4629	779.31099	56.686533	2934.6395	3158.2864

t Test

ABD2-YFP + CFP-A2-ABD2-YFP
Assuming unequal variances

Difference	481.182	t Ratio	5.758655
Std Err Dif	83.558	DF	290.787
Upper CL Dif	645.638	Prob > |t|	<.0001*
Lower CL Dif	316.727	Prob > t	<.0001*
Confidence	0.95	Prob < t	1.0000

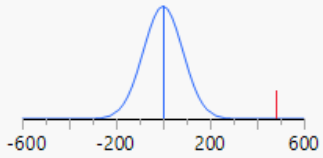

Supplemental Table 13. Relates to **Supplemental Figure 13A.** Co-expression of CFP-WPRA2 with ABD2-YFP does not decrease FABD2-YFP intensity **(Site B)**

Means and Std Deviations

Level	Number	Mean	Std Dev	Std Err Mean	Lower 95%	Upper 95%
ABD2-YFP	127	7712.9496	3592.3209	318.76693	7082.1192	8343.78
ABD2-YFP + CFP-A2	190	8774.6089	3868.2501	280.63236	8221.0349	9328.1829

t Test

ABD2-YFP + CFP-A2-ABD2-YFP
Assuming unequal variances

Difference	1061.66	t Ratio	2.499809
Std Err Dif	424.70	DF	283.4772
Upper CL Dif	1897.62	Prob > |t|	0.0130*
Lower CL Dif	225.70	Prob > t	0.0065*
Confidence	0.95	Prob < t	0.9935

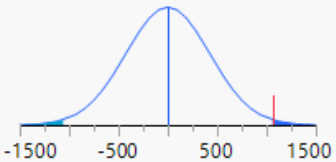

Supplemental Table 14. Relates to **Supplemental Figure 13B.** Co-expression of CFP-WPRA2 with ABD2-YFP does not decrease FABD2-YFP intensity

Means and Std Deviations

Level	Number	Mean	Std Dev	Std Err Mean	Lower 95%	Upper 95%
ABD2-YFP	127	3.0695412	1.3163422	0.1168065	2.8383846	3.3006978
ABD2-YFP + CFP-A2	189	2.8635325	1.0590525	0.0770347	2.7115689	3.015496

t Test

ABD2-YFP + CFP-A2-ABD2-YFP
Assuming unequal variances

Difference	-0.20601	t Ratio	-1.47231
Std Err Dif	0.13992	DF	230.2504
Upper CL Dif	0.06968	Prob > |t|	0.1423
Lower CL Dif	-0.48170	Prob > t	0.9288
Confidence	0.95	Prob < t	0.0712